



HAL
open science

Sea Ice Remote Sensing-Recent Developments in Methods and Climate Data Sets

Stein Sandven, Gunnar Spreen, Georg Heygster, Fanny Girard-Ardhuin,
Sinéad L. Farrell, Wolfgang Dierking, Richard A. Allard

► **To cite this version:**

Stein Sandven, Gunnar Spreen, Georg Heygster, Fanny Girard-Ardhuin, Sinéad L. Farrell, et al.. Sea Ice Remote Sensing-Recent Developments in Methods and Climate Data Sets. *Surveys in Geophysics*, 2023, 10.1007/s10712-023-09781-0 . hal-04204022

HAL Id: hal-04204022

<https://hal.science/hal-04204022>

Submitted on 4 Jan 2024

HAL is a multi-disciplinary open access archive for the deposit and dissemination of scientific research documents, whether they are published or not. The documents may come from teaching and research institutions in France or abroad, or from public or private research centers.

L'archive ouverte pluridisciplinaire **HAL**, est destinée au dépôt et à la diffusion de documents scientifiques de niveau recherche, publiés ou non, émanant des établissements d'enseignement et de recherche français ou étrangers, des laboratoires publics ou privés.



Distributed under a Creative Commons Attribution 4.0 International License



Sea Ice Remote Sensing—Recent Developments in Methods and Climate Data Sets

Stein Sandven¹ · Gunnar Spreen² · Georg Heygster³ · Fanny Girard-Ardhuin⁴ · Sinéad L. Farrell⁵ · Wolfgang Dierking^{6,7} · Richard A. Allard⁸

Received: 30 September 2022 / Accepted: 15 February 2023 / Published online: 3 April 2023
© The Author(s) 2023

Abstract

Sea ice monitoring by polar orbiting satellites has been developed over more than four decades and is today one of the most well-established applications of space observations. This article gives an overview of data product development from the first sensors to the state-of-the-art regarding retrieval methods, new products and operational data sets serving climate monitoring as well as daily operational services including ice charting and forecasting. Passive microwave data has the longest history and represents the backbone of global ice monitoring with already more than four decades of consistent observations of ice concentration and extent. Time series of passive microwave data is the primary climate data set to document the sea ice decline in the Arctic. Scatterometer data is a valuable supplement to the passive microwave data, in particular to retrieve ice displacement and distinguish between firstyear and multiyear ice. Radar and laser altimeter data has become the main method to estimate sea ice thickness and thereby fill a gap in the observation of sea ice as an essential climate variable. Data on ice thickness allows estimation of ice volume and masses as well as improvement of the ice forecasts. The use of different altimetric frequencies also makes it possible to measure the depth of the snow covering the ice. Synthetic Aperture Radar (SAR) has become the work horse in operational ice observation on regional scale because high-resolution radar images are delivered year-round in nearly all regions where national ice services produce ice charts. Synthetic Aperture Radar data are also important for sea ice research because the data can be used to observe a number of sea ice processes and phenomena, like ice type development and sea ice dynamics, and thereby contribute to new knowledge about sea ice. The use of sea ice data products in modelling and forecasting services as well as in ice navigation is discussed. Finally, the article describes future plans for new satellites and sensors to be used in sea ice observation.

Keywords Polar regions · Sea ice · Climate · Satellite remote sensing · Modelling

✉ Stein Sandven
stein.sandven@nersc.no

Article Highlights

- The reduction of Arctic sea ice is documented by passive microwave data from 1972 and radar altimeter data from 1993
- Sea ice volume export in Fram Strait, derived from ice drift and ice thickness, has decreased in the last three decades
- Synthetic Aperture Radar from Sentinel has become an operational observing system, providing daily data for sea ice research and services

1 Introduction

Sea ice covers the polar oceans in both hemispheres and is characterized by a large seasonal variability. Sea ice is an important component of the climate system because it has a high surface albedo compared to open water, together with the polar surface water it insulates the relatively warm ocean from the cold atmosphere, and it forms a barrier to the exchange of momentum and gases such as water vapor and CO₂ between the ocean and atmosphere. Regional climate changes affect the sea ice characteristics and those changes can feedback on the climate system, both regionally and globally. Sea ice has also important impact on the marine ecosystems and imposes restrictions on shipping and offshore operations in the polar regions.

The surface waters of the polar oceans freeze seasonally to form a layer of sea ice which varies in thickness from centimeters to meters. Sea ice growth and melt are governed by both thermodynamic and dynamic processes which lead to thickening and thinning. New ice, from millimeters to centimeters thick, lies very close to local sea level. As new ice floes consolidate and raft together, their thickness increases, and additional growth then occurs mainly at the bottom of the ice through accretion processes. When the ice pack diverges due to surface winds and/or ocean currents, leads can be formed where new ice can grow. Firstyear, or seasonal ice, which is formed during one winter, is typically between 0.3 and 2 m thick. Its growth and decay in the marginal ice zone causes large seasonal variations in total sea ice extent. Multiyear ice, which has survived one or more melt seasons, ranges in thickness from approximately 2–5 m and has a rough surface with hummocks and ridges formed through ice convergence. During the winter sea ice accumulates snow, which may thaw during the summer melt season to form slush and melt ponds atop the ice. Sea ice thickness together with its overlying snow controls ocean-ice-atmosphere exchanges of heat, momentum and gases at the ocean's surface.

Systematic and long-term observations of the major sea ice variables is only possible using past, present and future satellite Earth Observation (EO) data. Sea ice data from satellites has been collected for almost five decades, starting with the first passive microwave Nimbus-5 satellite Electrically Scanning Microwave Radiometer (ESMR) data in 1972. Sea ice observation has been one of the most successful applications of EO data in climate change studies as well as in other polar research topics. Several sensors and retrieval methods have been developed and successfully utilized to measure sea ice area, concentration and drift (e.g., Lavergne et al. 2019) Other sea ice parameters of importance for climate research are thickness, albedo, snow cover, temperature, duration of the melting season, amount of leads/polynyas and volume of ridges (e.g., GCOS 2016). Remote sensing can contribute to retrieving quantitative measurements of most

of these variables, even though the Global Climate Observing System (GCOS) defines sea ice in general as one Essential Climate Variable (ECV). For climate change studies it is generally accepted that the most important and mature variables, where quantitative retrievals have been obtained over several decades, are ice extent (area), ice thickness, and ice drift (<https://gcos.wmo.int/en/essential-climate-variables/sea-ice/>).

Through the Copernicus program, a series of Sentinel satellites have been launched since 2014 delivering data for monitoring the global environment (<https://www.copernicus.eu/en/about-copernicus>). The Sentinels have increased the amount of sea ice data significantly, stimulating research to develop new derived sea ice products. For global monitoring of sea ice, passive microwave, scatterometer and altimeters will continue to deliver data from various satellite programs. In addition to the satellite data, it is important to collect relevant in situ measurements for validation of the satellite products and support further sea ice research.

A historical overview of sea ice observations in the Arctic, including a description of data from various satellite programs, is provided in a recent book by Johannessen et al. (2020), and this article is an update of recent development of sea ice retrieval methods and data sets from satellite sensors.

The article is organised into the following sections: Passive microwave radiometry is described in Sect. 2, Scatterometry in Sect. 3, Radar and laser altimetry in Sect. 4, Synthetic Aperture Radar in Sect. 5, modelling and application of sea ice data products in services in Sect. 6, and support to ice navigation in Sect. 7. The conclusions and future outlook are presented in Sect. 8.

2 Passive Microwave Radiometry

Since the early days of satellite remote sensing, passive microwave sensors have played a key role in global sea ice observation. The first passive microwave sensor in space was the Electrically Scanning Microwave Radiometer (ESMR) on NASA's Nimbus 5 observing at 37 GHz (1972–1977). The Scanning Multichannel Microwave Radiometer (SMR) on Nimbus 7 operated 1978–1987 at three frequencies, two with dual polarization, allowing discrimination between ice types first-year and multiyear ice, and a correction for weather influences. The global observations with spaceborne radiometers continued with the sequence of seven Special Sensor Microwave Imager (SSM/I) on the Defense Meteorological Satellite Program (DMSP) satellites (1991–2020) and with the Special Sensor Microwave Imager / Sounder (SSMIS) sensor on four more DMSP satellites from 2003 to today observing sea ice at 19, 37 and near 90 GHz.

Currently the global passive microwave observations of sea ice mainly depend on the instruments AMSR-E (2002–2011) and AMSR2 (2012-present) on the AQUA and GCOM-W platforms, respectively. Because of the larger antenna reflector diameters of 1.6 m (AMSR-E) and 2.0 m (AMSR2), they offer data of much higher resolution than the SSM/I and SSMIS instruments with only 0.64 m diameter reflectors. The average resolution at the various AMSR2 frequencies are 49 km for 6.93 GHz and 7.3 GHz, 33 km for 10.65 GHz, 18 km for 18.7 GHz, 15 km for 23 GHz, 10 km for 36.5 GHz and 4 km for 89.0 GHz. All described radiometers use a conical scan scheme so that they observe at the same incidence angle around 50° where the information obtained at vertical and horizontal polarization direction is highest. References to the brightness

temperature data sets of these satellites are given in Barry and Gan (2011). In the following sub-sections a short overview of the most important sea ice parameters obtained from microwave radiometry is given.

2.1 Sea Ice Concentration and Sea Ice Extent

Sea ice concentration (SIC) is defined as the percentage of ocean surface covered by sea in one cell of a gridded map. The retrieval algorithms use passive microwave data from several channels with different frequencies or polarizations. A number of different algorithms have been developed over the years, most of them use data from the 19 and 37 GHz channels (e.g. Lavergne et al. 2019). The fundament of the algorithms is described in Barry and Gan (2011) or Long and Ulaby (2015). The developments since then have focused on (1) reduce and quantify the error, (2) improve the spatial resolution and (3) retrieving several geophysical parameters simultaneously. The comparative study by Ivanova et al. (2015) demonstrated the tradeoff between goal (1) and (2): at low microwave frequencies, e.g. 6 GHz, the atmospheric influence is low so that SIC retrieval has low errors, but also the resolution is low (see last section), whereas at high frequencies, i.e. near 90 GHz, the resolution is higher, but the influence of atmospheric water vapor and clouds is stronger and more difficult to separate from the surface signal. Regarding aspect (3) on retrieving several geophysical parameters simultaneously from the complete set of brightness temperatures at all frequencies and polarizations, the use of Optimal Estimation Methods (OEM) shows promising results. For example, Scarlat et al. (2020) retrieve seven surface and atmosphere parameters (including ice concentration, ice type, water vapor etc.) from joint AMSR2 and SMOS microwave radiometer observations.

The horizontal dimension of the sea ice cover is typically described by the sea ice area or the sea ice extent, which is derived from sea ice concentration. For the sea ice area, the area of the sea ice pixels of an Arctic or Antarctic sea ice map are summed, each weighted by its SIC. The second measure, the sea ice extent, only counts each pixel with SIC > 15%. Pixels with SIC values below 15% are ignored. The sea ice extent is less sensitive to uncertainties in retrieval, especially when comparing results from different retrieval algorithms and in summer when the errors in SIC retrieval are higher. Examples of maps of sea ice area, ice type, thin ice thickness, and snow on sea ice for the Arctic and Antarctic, are presented in Fig. 1 and Fig. 2. An example of time series of sea ice extent over five decades is shown in Fig. 3. This time series covers almost 5 decades and is the longest climate data record from satellite sensors and is one of the key data sets for documenting climate change in the Arctic.

2.1.1 Reducing and Quantifying the Retrieval Error

Passive microwave remote sensing of sea ice made significant progress through ESA's Climate Change Initiative (CCI) from 2012 to 2018 where updated data sets on ice concentration (Lavergne et al. 2019) were produced based on improved retrieval algorithms. The updated data sets offer two distinct advantages. First, all records provide quantitative information on uncertainty at every grid point and every time step, which is a prerequisite for assimilating the data into circulation models. Second, the data sets are based on dynamic reference brightness temperatures of open water and sea ice (tie points). They are based on a time window of 15 days total around the observation time to capture the time evolution of surface characteristics of the ice cover and

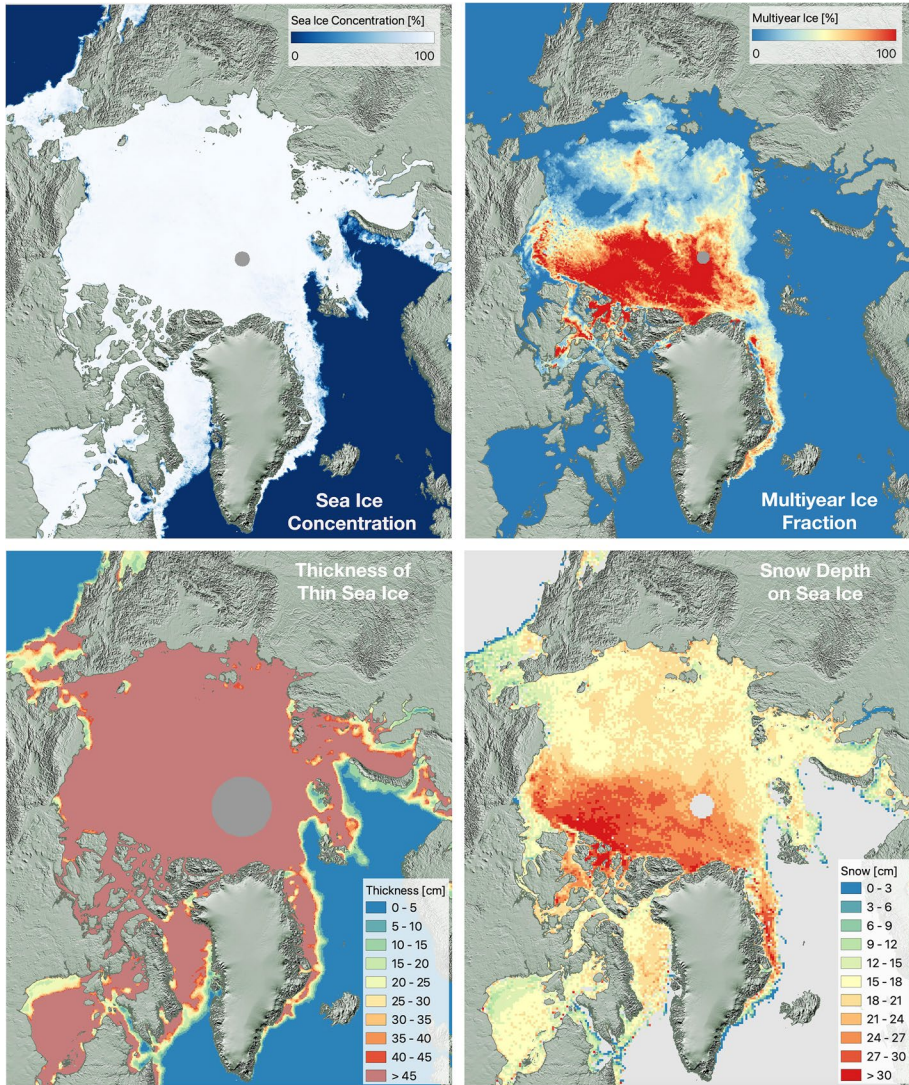


Fig. 1 The Arctic on 5 March 2021 observed by satellite microwave radiometers. Top left: Sea ice concentration (ASI) from AMSR2 (Spreen et al., 2008); Top right: Multiyear ice fraction from combined AMSR2 and ASCAT (Ye et al. 2016); Bottom left: Thickness of thin sea ice from merged SMAP and SMOS (Patilea et al. 2019); Bottom right: Snow depth on sea ice from AMSR2 (Rostovsky et al. 2018)

to accommodate potential calibration differences between satellite missions. The core of the algorithm is a blend between the bootstrap frequency mode (BFM) algorithm, and the Bristol (BRI) algorithm. These algorithms were found to performed best at low (BFM) resp. high SIC (BRI) values in the comparative study by Ivanova et al. (2015). The most up-to-date algorithms, presented by Lavergne et al. (2019) represent further

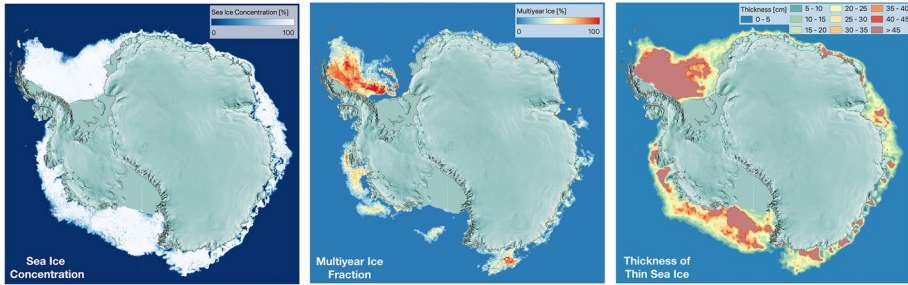


Fig. 2 The Antarctic on 1 April 2020 observed by satellite microwave radiometers. Left: Sea ice concentration (ASI) from AMSR2 (Spreen et al. 2008); Middle: Multiyear ice fraction from combined AMSR2 and ASCAT (Melsheimer et al. 2022); Right: Thickness of thin sea ice from merged SMAP and SMOS (Patilea et al. 2019; Mchedlishvili et al. 2022)

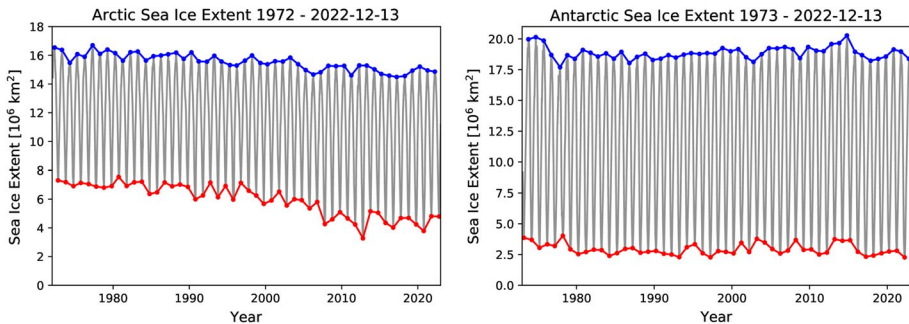


Fig. 3 Sea ice extent for the Arctic (left) and Antarctic (right) from 1972 to 2022 based on combined ESMR, SMMR, SSM/I-SSMIS, and AMSR-E/2 satellite data. Grey lines show monthly data and thus the seasonal cycle, while blue and red lines show the development of the winter maximum and summer minimum ice extent, respectively

development of previous algorithms with focus on producing consistent climate data records for sea ice.

2.1.2 Improving Resolution

Based on existing passive microwave data, the only way to increase the horizontal resolution is using observations at higher frequencies, first suggested by Svendsen et al. (1987). A widely used example is the ASI algorithm (Spreen et al., 2008; Figs. 1, 2). It relies on the brightness temperature difference between horizontally and vertically polarized data at 89 GHz. At this frequency, the atmospheric influence from water vapor and clouds on the brightness temperature cannot be ignored. It is reduced by so-called weather filters which screen out spurious ice concentrations over open water. They rely on the normalized brightness temperature differences between 23 and 37 GHz for water vapor and 18 and 37 GHz for cloud liquid water.

Two methods for correcting the brightness temperatures have been developed, one is based on atmospheric model data like the ECMWF re-analysis (Lu et al. 2018). The other is based on optimal estimation of the atmospheric parameters obtained from the brightness

temperature observations of the same instrument and at the same time, but at lower frequencies (Lu et al. 2022). With this method, the influence of cloud liquid water can be better compensated for, which could not be done when correcting with atmospheric model data alone. Another way to increase the resolution is using a larger antenna reflector, see Sect. 8.

2.2 Sea Ice Type

Different sea ice types are defined by the age and stage of development according to WMO Sea Ice Nomenclature (WMO, 2014). From passive microwave data it is possible to separate firstyear ice and multiyear ice, i.e. ice that survived at least one summer melt. The separation is possible because passive microwave data are sensitive to properties that are different for the two ice types. These include salinity, temperature, density, surface roughness and snow cover properties. One major difference is the desalination of the ice happening during summer melt, which makes multiyear ice less saline and allows deeper penetration of microwaves into the ice compared to firstyear ice. Furthermore, multiyear ice is on average more deformed, has higher surface roughness, and a higher snow cover. All these processes increase microwave scattering for multiyear ice compared to firstyear ice, i.e., reduces its emissivity and thus brightness temperature T_B . Usually the normalized difference (gradient ratio, e.g. $GR_{37,19} = \frac{T_B(37V) - T_B(19V)}{T_B(37V) + T_B(19V)}$) between two frequencies (19 and 37 GHz) is employed to separate sea ice types in microwave radiometry (e.g., Cavalieri et al. 1984).

A recent development is to merge microwave radiometer and scatterometer data to improve the discrimination between firstyear and multiyear ice (e.g. Ye et al. 2016; Melsheimer et al. 2022). Both radiometer and scatterometer data can provide ice type fractions at spatial resolutions of 10 km and lower. This makes them useful for climate studies, documenting the strong decline in the old, thick multiyear ice of about $13 \pm 2\%$ per decade (IPCC, 2021). Examples of merging are shown in Figs. 1, 2, while the methods are further described in Sect. 3.

The main uncertainties in ice type separation are often found in the marginal ice zone, where smaller floes, more ice deformation or pancake ice, which has high surface roughness and more edges, increase surface roughness of young and first-year ice types and thus can lead to misclassification. By taking the ice history into account such misclassifications can be reduced (e.g., Ye et al. 2016).

2.3 Thickness of Thin Sea Ice

Thin sea ice develops during the freeze-up season over large areas in the marginal ice zone and coastal areas of the polar seas. During the cold season thin ice also develops in leads and coastal polynyas. In areas of thin ice, with thickness varying from a few cm to half a meter, the salt fluxes generated by freezing and heat fluxes from ocean to atmosphere are important process affecting the weather and ocean circulation in the polar regions. Algorithms for retrieval of thin sea ice thickness (SIT) from passive microwave data was developed using the L-band (1.4 GHz) on ESA's SMOS mission. At L-band the full microwave penetration into the sea ice is used to retrieve SIT of up to 0.5–1.0 m (Tian-Kunze et al. 2014; Huntemann et al. 2014), where the maximum retrievable SIT depends on ice temperature and salinity. Since 2015, NASA's SMAP mission has provided similar passive microwave data at the same frequency. Two independent methods for combining brightness

temperature (TB) data from SMOS and SMAP have been suggested by Schmitt and Kaleschke (2018) and Patilea et al. (2019). Examples of thin ice maps are shown in Figs. 1, 2. The combination of thin sea ice thickness from passive microwave observations with thicker sea ice retrievals from altimeters is described in Sect. 4.

2.4 Snow on Sea Ice

The snow depth on sea ice strongly determines its thermal insulation and thus the energy transfer between ocean and atmosphere in polar regions. Snow depth is therefore an important input parameter to thermodynamic models of sea ice. Data on snow depth is also important for shipping because thick snow cover produce friction and affects the speed icebreakers when they navigate in sea ice covered (Section 2.2).

The amount of snow on top of the sea ice changes its microwave scattering properties. Thus, similar to ice type, most snow depth retrievals utilize the different scattering properties at two or more different microwave frequencies. For example, Markus and Cavalieri (1998) used an empirical relationship of the $GR_{37,19}$ gradient ratio (see equation in Section 2.2) to retrieve snow depth. This retrieval is limited to < 50 cm snow and to first-year ice because the GR varies also with the multiyear ice fraction (Section 2.2). More recent retrievals (e.g., Rostosky et al. 2018) also employed lower frequencies, e.g. at 7 GHz, to extend the snow depth data to multiyear ice (Fig. 1). At 1.4 GHz (L-band) the insulating effect of snow and thus its influence on the snow-ice interface temperature and brine volume fraction in the ice can be used to retrieve the snow depth (Maaß et al. 2013). Snow depth retrievals are influenced by grain size variations, snow wetness (Markus et al. 1998), salinity in the snow, and often under-estimates snow depth for rough sea ice (e.g. Kern et al. 2011).

2.5 Sea Ice Motion

Sea ice motion can be retrieved by detecting and tracking structures in the ice cover in a pair of consecutive overlapping microwave radiometer images. Patterns found in the brightness temperature maps of the first day are identified by cross-correlation methods in the observations of the later day, which usually are obtained one to three days apart (e.g., Laverne et al. 2010). This motion is often defined as ice displacement, because it only provides a start point and end point of the motion. The spatial resolution is about 50 km because of the resolution of the passive microwave data. Long-term time series of ice displacement are important in ice dynamics and climate studies (Spreen et al. 2011). Further discussion of sea ice displacement is presented in Sects. 3, 4.

2.6 Sea Ice Change and Global Climate

The reduction of Arctic sea ice is one of the strongest climate change signals observed globally today. With an now almost 50-year long time series (Fig. 3) observations from satellite microwave radiometers are the primary data source for monitoring sea ice extent in the polar regions. Long-term in-situ observations of sea ice are sparse, limited to a few locations and not sufficient to build a consistent climate record of the sea ice extent. Analysis of passive microwave data shows the following trends (IPCC 2021, Stroeve et al. 2014; Spreen et al. 2011).

- a decrease of Arctic sea ice extent of annually $4\% \pm 1\%$ per decade
- a decrease of the old, multiyear sea ice of $13\% \pm 2\%$ per decade
- an increase of melt season length of 5 ± 1 days per decade
- an increase of sea ice drift speed of $11\% \pm 1\%$ per decade
- Antarctic sea ice area shows no significant trend due to regionally opposing trends

The strong reduction in Arctic sea ice is directly coupled with the amplified warming of the near surface atmosphere (more than three times the global average) and ocean temperatures in the Arctic. Some of the important feedbacks for this amplified sea ice melt and Arctic climate warming are the ice-albedo feedback during summer, reduced insulation between ocean and atmosphere due to sea ice thinning during winter, and the lapse-rate feedback in the atmosphere over sea ice. However, these sea ice and climate changes are not limited to polar regions. Studies show coupling and teleconnections between polar regions and mid-latitudes and associated atmospheric circulation and extreme weather changes. For example, a reduced temperature gradient between the Arctic and mid-latitudes because of the faster warming Arctic will impact atmospheric circulation. One example would be the stronger meandering polar jet stream, which would lead to both more cold-air outbreaks from the Arctic to mid-latitudes as well as more warm-air intrusions to the Arctic. The strength of the coupling, however, to sea ice loss is still under discussion.

2.7 In-Situ Observations for Evaluation and Process Understanding

The microwave brightness temperatures observed by the satellite sensors need to be connected with the wanted geophysical variables, such as ice concentration, ice area or thickness. For this the emission and scattering of microwaves with sea ice, snow, and the atmosphere need to be understood. Many fundamental on-ice microwave radiometer measurements were obtained during the early satellite record time period, e.g., the NORSEX and MIZEX campaigns from 1979 to 1984 (e.g., Svendsen et al. 1987).

Recently the one-year long MOSAiC expedition provided the opportunity to obtain measurements of the “New Arctic” with a strongly reduced sea ice cover, which are critically needed for a better process understanding and updated parametrizations in climate models. The research icebreaker *Polarstern* was frozen-in and drifted with the sea ice in the Central Arctic from October 2019 to September 2020 (Nicolaus et al. 2022). During the drift, 14 remote sensing instruments, similar to their counterparts in space, were operated on the MOSAiC ice floe. These included six microwave radiometers, operating in the frequency range from 0.5 to 89 GHz, observing the surface brightness temperature collocated with an extensive snow and ice geophysical measurement program. The temporal development of microwave emission throughout the seasons was monitored and connected with environmental changes like temperature, snow grain size, salinity, etc., to obtain a better understanding of the interaction of microwaves with snow and ice. In turn, the new knowledge can be incorporated in satellite retrieval algorithms and especially used for better uncertainty assessments. For example, a warm air intrusion event in April 2020, i.e., still under winter conditions, and associated snow changes caused a strong ($> 10\%$) underestimation of sea ice concentration by most satellite retrievals (Krumpfen et al. 2021), which in future, with the help of the MOSAiC measurements, potentially can be detected and corrected.

The current passive microwave observations allow retrieval of many more parameters than described in this article, among them (1) sea ice parameters: sea ice edge, start, end

and length of melt season, and sea ice surface temperature, (2) open ocean parameters: sea surface temperature, sea surface salinity, ocean surface wind vector, and (3) atmospheric precipitation, liquid water path and total water vapor column, and (4) land parameters: terrestrial snow area, lake surface water temperature, soil moisture, vegetation index, and surface water fraction.

3 Scatterometry

A scatterometer is a radar transmitting pulses of microwaves towards the surface of the Earth which measures how much of the energy is reflected back to the instrument. The instrument was originally designed for global ocean wind observations, and wind monitoring has been the main purpose of the scatterometer satellites since they started to operate 30 years ago. In addition, scatterometer data has also demonstrated to be very useful in observation of sea ice. The scatterometers onboard polar orbit satellites provide almost full data coverage every day over the sea ice areas in both Arctic and Antarctica, independent of weather and light conditions.

A series of C- and Ku-band scatterometers have been launched since the 1990's by the major space agencies in USA, Europe and Asia. Historically, scatterometers of the European Space Agency (ESA) used the C-band (5 GHz), while the National Aeronautics and Space Administration (NASA) used the Ku-band (14 GHz), which has different sensitivity to wind variations, rainfall and other atmospheric effects compared to C-band (Liu, 2003). Most of the scatterometers are in polar orbits and provide data for use in sea ice monitoring. Scatterometer data are useful to estimate sea ice displacement, to separate between sea ice and open ocean, and to discriminate between firstyear and multiyear ice. A useful description of scatterometry and summary of past, present and future scatterometer satellites is found in <https://www.coaps.fsu.edu/scatterometry/about/overview.php>.

3.1 Sea Ice Displacement

Since the 1990's, several methods have been developed to retrieve sea ice displacement from scatterometer data provided daily over the ice-covered oceans. Retrieval of ice displacement can be done during the cold period from October to April. During the melt season, the retrieval methods are not reliable because feature recognition is more difficult. The ice displacement is estimated at spatial scale of tens of km and time intervals from one to six days. All the retrieval methods assume that the structures tracked have a spatial dimension higher than the pixel resolution. Several methods have been tested including wavelet analysis, which is similar to Fourier transform in both time and frequency (Liu et al. 1999), and methods mainly based on tracking common features in pairs of images. The Maximum Cross Correlation is a commonly used method to estimate translatory displacement of ice structures (e.g., Emery et al. 1997). The method has been further developed by, e.g., Lavergne et al. (2010).

Lagrangian trajectory data has been provided from drifting ice buoys since the early 1990s operated under the International Arctic Buoy Programme where new buoys are deployed every year providing near real-time meteorological and sea ice data (https://iabp.apl.uw.edu/overview_history.html). The trajectory data are applied for validation of ice displacement data from both active and passive microwave data. Displacement datasets are derived from scatterometer or radiometer observations separately, or as merged data sets

Fig. 4 Map of ice displacement vectors and mean sea ice volume flux in the Arctic for the winter 2016–2017. From Ricker et al (2018)

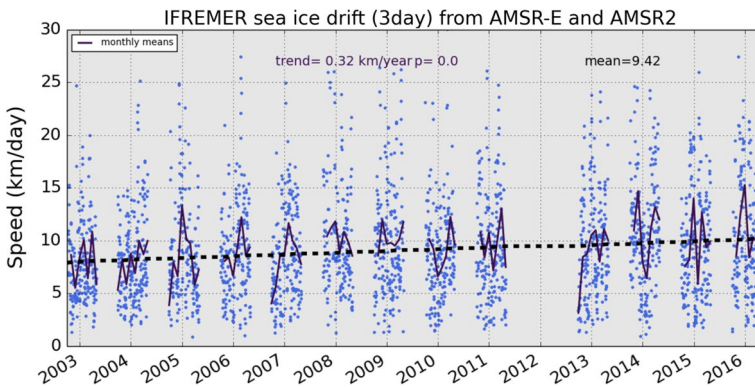
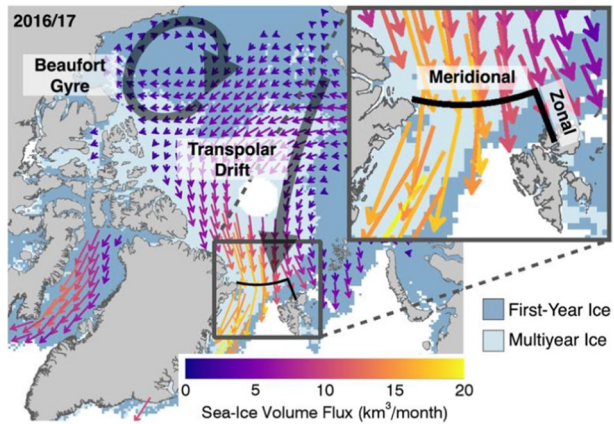


Fig. 5 Time series of sea ice drift north of Svalbard obtained during the freezing period each year. The data shows a positive trend in sea ice speed of 032 km per year from 2003 to 2017. From Itkin et al (2017)

from both sensors. By merging scatterometer data with passive microwave data the spatial resolution of the ice displacement vectors can be increased by $\approx 15\%$ and the length of the retrieval period from autumn to spring can be extended. Studies of merging data from these sensors have shown that up to 90% of the displacement vectors retrieved during the cold months provided realistic estimates of the ice displacement (Girard-Arduin and Ezraty 2012).

The ice displacement maps produced from scatterometer data only have a grid resolution of about 60 km. By including passive microwave radiometer data from AMSR the resolution is increased to 30 km grid size, but with more data gaps and fewer estimated vectors during the freezing period. During the summer months the retrieval of ice displacement vectors is not feasible due to the melting of sea ice which makes feature recognition difficult. An example of sea ice displacement vectors and volume flux in the whole Arctic is shown in Fig. 4. An example of a time series of ice drift north of Svalbard is shown in Fig. 5.

The ice displacement data sets and derived products are made available for the scientific community and operational monitoring and forecasting services on regular basis by processing and archiving centers (e.g., <https://cersat.ifremer.fr/>, <https://nsidc.org/home>, [Springer](https://</p>
</div>
<div data-bbox=)

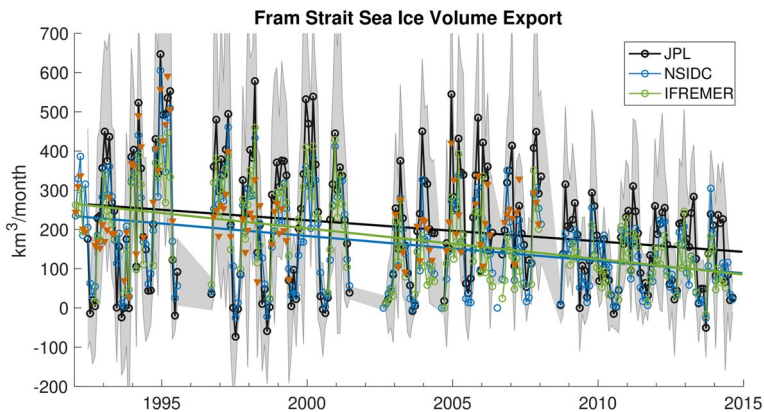


Fig. 6 Time series of Fram Strait volume export estimated from three different sea ice drift data sets covering the period 1992–2015. From Spreen et al. (2020)

www.eumetsat.int/osi-saf) and numerous research institutes. One example of a derived product is sea ice volume exiting the Arctic basin through the Fram Strait (Fig. 6). Sea ice displacement data are also used for studying ice-ocean-atmospheric processes. Examples are provided by Itkin et al. (2017) who studied the impact of winter storms on the Arctic sea ice distribution, Ricker et al. (2018) showed that sea ice thickness anomaly can be explained by a sea ice displacement anomaly, and Bi et al. (2019) evaluated the Baffin Bay sea ice inflow and outflow since the 1970's. Time series of sea ice displacement have also been analysed for long-term trend as a climate indicator (e.g., Rampal et al. 2009). The data are of interest in model assimilation with an impact of modelled displacement but also on thickness estimate. The datasets are also used in ship routing and by insurance companies and oil companies to support sea transport and operations in the Arctic.

3.2 Sea Ice Type

Backscatter data from scatterometers depend on both sensor characteristics (e.g., frequency, polarisation, incidence angle) and sea ice properties (e.g., surface roughness, salinity, snow and porosity). Firstyear and multiyear ice can be separated during the cold season based on different backscatter, while in the melt season the backscatter is similar for both ice types because the surface is dominated by wet snow and melt ponds. In the marginal ice zone, the separation of ice types is also difficult because waves and swell tend to break up the ice into smaller floes with rough surface leading to high backscatter for both firstyear and multiyear ice.

Several techniques have been developed to separate firstyear and multiyear ice, including use of passive microwave data (see Sect. 2). Kwok et al. (2004) used a backscatter threshold in analysis of QuikSCAT Ku-band data, supported by high-resolution SAR data. Swan and Long (2012) demonstrated use of a time-dependent threshold in QuikSCAT data, validated with ice charts and completed with ASCAT data (Lindell and Long 2016). Recently, Li et al. (2016) showed that also HY-2A can be used to discriminate between multiyear and firstyear ice in Ku-band data. A Bayesian method has been applied to backscatter data from several scatterometer data sets from 1992 to 2018, to separate firstyear,

second-year and multiyear ice and show the evolution of these ice types over 25 years (Belmonte Rivas et al. 2018).

Data in Ku-band are more sensitive to volume scattering of multiyear ice, offering a better method to separate it from firstyear ice compared to use of C-band data. Traditionally, C- and Ku-band data were produced by different satellites. Therefore, it is a challenge to establish homogeneous time series over several decades where multiyear and firstyear ice are separated. However, several of the planned scatterometers will have a combination of C- and Ku-band. These scatterometers will continue to be operated under Eumetsat and NOAA’s polar programmes, providing C- or Ku band data primarily for ocean wind observations, but also for sea ice. Other scatterometer satellites have been launched by China (HY-2 satellites) and the China-France Oceanography Satellite (CFOSAT). These programmes will ensure that scatterometer data will be available for sea ice observations in the coming years.

4 Altimetry

4.1 Background

Spaceborne altimeters have been profiling the Arctic Ocean since 1991 beginning with the ERS-1 satellite, measuring polar ocean height to a latitudinal limit of 81.5° N (Peacock and

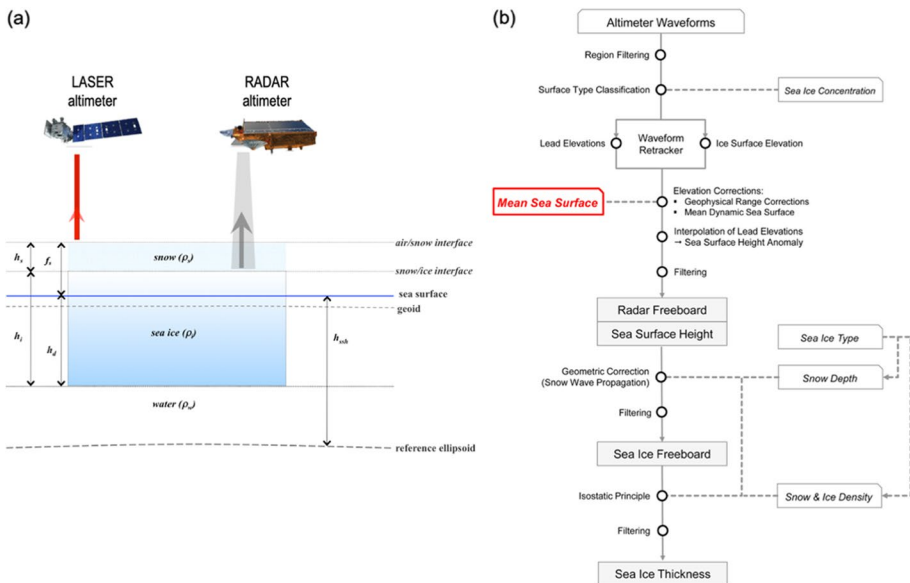


Fig. 7 Idealized schematics illustrating **a** the satellite laser and radar altimeter freeboard measurement concept for a snow-covered sea ice floe in hydrostatic equilibrium, where sea ice thickness (h_i), snow thickness (h_s), laser-derived snow freeboard (f_s), sea ice draft (h_d) and sea surface height (h_{ssh}) are shown, and **b** a flow chart describing the classic processing chain by which freeboard and thickness are deduced from satellite radar altimeter waveform measurements of surface height. Modified from Farrell et al. (2009) and Skourup et al. (2017)

Laxon 2004). Laxon et al. (2003) described the use of conventional Ku-band radar altimeters operating at 13.8 GHz on ERS-1 and ERS-2 to determine sea ice freeboard and estimate ice thickness in the Arctic by using auxiliary information on snow depth, ice, water, and snow density and assuming local hydrostatic equilibrium (Fig. 7).

Envisat, launched in March 2002, also facilitated coverage of the Arctic to 81.5° N by following a similar orbit configuration to the ERS-2 satellite, flying in a 35-day exact repeat orbit. Envisat carried a nadir-looking, conventional, pulse-limited radar altimeter, operating at two frequencies: 13.575 GHz (Ku Band) and 3.2 GHz (S band). Since the radar altimeter on Envisat was similar to that employed on the earlier ERS satellites the methods described in Laxon et al. (2003) were also used to derive sea ice thickness from Envisat data, albeit with a small additional correction for the radar travel time through the snow pack (Giles et al. 2008a, Hendricks 2018).

A major limitation of the ERS-1/2 and Envisat satellite radar altimeter datasets, however, is that only partial observations exist for the Central Arctic due to satellite orbit constraints which limit coverage to 81.5° N. Since the early 2000s, NASA and ESA committed to obtaining measurements of changes in sea ice thickness via the use of high-resolution satellite laser and radar altimeters dedicated to polar observations. Although these missions are part of a global suite of satellite altimeters (International Altimetry Team 2021), crucially their orbital inclinations are designed to provide extensive coverage of both polar oceans.

Launched in 2003, NASA's Ice, Cloud and land Elevation Satellite (ICESat) mission presented the first opportunity to obtain high-resolution satellite laser altimeter data with coverage of the Arctic to 86°N latitude, in a 91-day exact repeat orbit with a 94° inclination. An additional area of Arctic sea ice $\sim 2 \times 10^6$ km² in size was thus observed by ICESat compared to ERS-1/2 and Envisat. The Geoscience Laser Altimeter System (GLAS) on ICESat provided high-resolution satellite laser altimeter data (~ 70 m footprints spaced at 172 m along track) with a height precision of ~ 2 cm over flat sea ice surfaces (Kwok et al. 2004). Observations were, however, hampered due to periodic measurement campaigns wherein laser operation periods lasted for only 33-day subcycles as a result of laser lifetime considerations. Between 2003 and 2006, laser operation periods occurred three times per year, and from 2007 to 2009 they occurred only twice a year so as to extend the life of the laser at the end of the mission.

During the same time period ESA launched CryoSat in 2005; however, the spacecraft was lost in a launch failure. Just five years later the program resumed with the successful launch of a replacement mission, CryoSat-2 in 2010. CryoSat-2 carries the SAR/Interferometric Radar Altimeter (SIRAL) instrument to determine precise and detailed surface topography along the satellite ground track at a higher spatial resolution than was previously possible with conventional, pulse-limited radar altimeters. SIRAL illuminates a footprint on Earth's surface approximately 0.3 km by 1.5 km along track and across track, respectively, which compares to footprint diameters of > 10 km on the earlier, pulse-limited radar altimeter missions (Laxon et al. 2013). With an orbital inclination of 92°, CryoSat-2 provides even more complete coverage of the polar regions than ICESat, up to a latitudinal limit of 88° N/S. CryoSat-2 operates a long, 369-day repeat period, but with a sub-cycle period of 29 days. At present CryoSat-2 had successfully completed 12 years of continuous observations on orbit.

SAR altimetry has led to considerable improvements in the measurement of freeboard, both in terms of spatial resolution and uncertainty. These data have allowed revisiting measurements made by previous low-resolution measurement (LRM) altimeters on Envisat and ERS-1/2 thanks to calibration techniques during common flight periods (Guerreiro

et al. 2017, Paul et al. 2018). This effort has made it possible to restore homogeneous series of pack ice thickness over nearly 3 decades (Bocquet et al. 2022).

In 2018, CryoSat-2 was joined by a sister satellite, NASA's ICESat-2, also operating with an orbital inclination of 92° , but with a 91-day exact repeat period. Although a follow-on to the ICESat mission, ICESat-2 operates the Advanced Topographic Laser Altimeter System (ATLAS), which uses a different detection strategy to GLAS on ICESat. ATLAS is a high-repetition-rate (10 kHz), multi-beam, 532 nm-wavelength laser altimeter that utilizes photon-counting techniques for surface detection (Markus et al. 2017). ATLAS has six laser beams, arranged in three sets of beam pairs, with spacing between sets of pairs ~ 3000 m apart, while each beam within a given pair is ~ 90 m apart, with footprints ~ 11 m in diameter. This multi-beam design configuration allows for surface slope detection on ice sheets, but also enhances sea ice freeboard determination by increasing the number of available height measurements across leads in the sea ice cover.

4.2 Sea Ice Thickness

Continuous monitoring of ice thickness has proved a more difficult task than measuring ice extent; while remote sensing techniques were available since the late 1970s to routinely map and monitor sea ice extent, it was two decades later before satellite altimeter techniques were developed to estimate ice thickness (Laxon et al. 2003). Until that time upward looking sonar was the most useful method to determine the regional and seasonal distributions of sea ice thickness in the Arctic, while in the Southern Ocean, knowledge was limited to sparse field observations of thickness (Giles et al. 2008b).

Estimating sea ice thickness in the Arctic and Southern Oceans from satellite altimeter data ultimately relies upon (1) discrimination between waveform returns from the sea surface (i.e., from areas of open water within the ice pack called leads) and those arising from the sea ice floes, and (2) the height of both these leads and sea ice floes. Accurate lead detection and precise measurement of the instantaneous sea surface height are equally crucial, and thus the processing approach for altimeter data collected over ice-covered waters is customized to discriminate leads from sea ice floes (Fig. 7). Briefly, waveform returns originating from leads (open water or thin ice) are specular in nature while those from ice floes are more diffuse (Peacock and Laxon 2004). The retracking methods developed in Peacock and Laxon (2004) and Giles et al. (2012) and applied to ERS-1/2 and Envisat data, respectively, have also been applied to CryoSat-2 data (Laxon et al. 2013). Lead waveforms are identified using a combination of criteria including the waveform pulse peakiness, leading edge width, and in the case of CryoSat-2 data the beam "stack standard deviation" (Laxon et al. 2013). The retracker for lead waveforms was a "Gaussian + exponential" function fit to the return waveforms (Giles et al. 2007), while waveforms originating from the open ocean are retracked using a more simplistic threshold retracker. On the other hand, lead surfaces in ICESat and ICESat-2 laser altimeter data are defined by the energy or photon rate of the return signal ("dark" leads return less energy/photons than "bright" ice floes) combined with characteristics of their surface elevation since leads are both level surfaces, with low standard deviation, less pulse spreading, and are lower in height than the surrounding ice floes (Kwok et al. 2004; Markus et al. 2017). Classification of leads and measurement of the height with both radar and laser altimeters therefore provide reference profiles of sea surface height over time (Fig. 7b).

Calculation of sea ice freeboard, f , that part of the ice floe which floats above the local sea surface, relies upon subtraction of the interpolated sea surface height from sea ice

height, typically applied per orbit in the along-track direction. As illustrated in Fig. 7a, in the case of laser altimeter retrievals, the freeboard measurement, f_s , is the height of the sea ice, plus accumulated snow, above the local sea surface, whereas at Ku-band wavelengths the radar signal is assumed to penetrate the snow cover, such that under cold, dry snow conditions reflections arise from the snow/ice interface and the freeboard measurement, f_i , is simply the height of the sea ice without snow (Laxon et al. 2013). When combined with knowledge of snow thickness, h_s , and assumptions about the density of snow, ρ_s , ice ρ_i , and sea-water ρ_w , freeboard can be used to infer sea ice thickness, h_i , assuming ice floes are in local hydrostatic equilibrium (Fig. 7). Since snow loading on sea ice is not directly measured, it frequently approximated using updated Warren et al. (1999) climatology. More recently, Garnier et al. (2021) and Zhou et al. (2021) have evaluated snow on sea ice model outputs such as NASA Eulerian Snow On Sea Ice Model (NESOSIM) (Petty et al. 2018), SnowModel-LG (Stroeve et al. 2020a, b) and DusT (Lawrence et al. 2018), as well as spatial measurements by passive radiometers (see Sect. 2.4) or dual-frequency altimetry (see Sect. 4.3). Sea ice thickness may hence be estimated from freeboard measurements by laser and radar altimeters, respectively, as

$$h_i = \frac{\rho_w}{\rho_w - \rho_i} f_s + \frac{\rho_s - \rho_w}{\rho_w - \rho_i} h_s \quad (4.1)$$

$$\text{and } h_i = \frac{\rho_w}{\rho_w - \rho_i} f_i + \frac{\rho_s}{\rho_w - \rho_i} h_s \quad (4.2)$$

Satellite altimeter-derived sea ice thickness climatologies for the Arctic Ocean, derived from single-mission averages of ice thickness during winter demonstrate the advances made in both spatial coverage and measurement resolution over the last three decades. Figure 8 demonstrates the impact of orbits optimized for viewing the polar regions and higher-resolution sampling of the surface to obtain improved spatial coverage and detail across the ice cover of the Arctic Ocean. Radar altimeter measurements can, however, produce higher relative thickness errors in regions of thin ice due to limitations in the achievable precision of lead height measurements (Sallila et al. 2019). By employing an optimal interpolation scheme, CryoSat-2 thickness estimates may be combined with thin ice (< 1 m) estimates derived from the ESA Soil Moisture Ocean Salinity (SMOS) L-Band radiometer instrument to obtain a merged multi-satellite thickness estimate (Fig. 8) that is valid across both thin and thick ice regimes (Ricker et al. 2017b). When combined with sea ice concentration derived from passive microwave radiometer observations, the blended CryoSat-2/SMOS record of ice thickness is used to indicate variability in sea ice volume (Fig. 9).

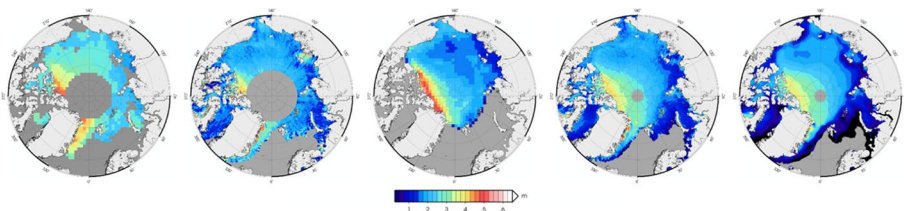


Fig. 8 Altimeter-derived sea ice thickness climatologies for the Arctic Ocean derived from ERS-1/2 (1993–2001), Envisat (2003–2011), ICESat (2004–2009), CryoSat-2 (2011–2020) and CryoSat-2/SMOS (2011–2020). Mission averages at the end of winter (April) are shown. Data sources: Laxon et al. (2003), Hendricks et al. (2018), Yi and Zwally (2009) and Hendricks et al. (2016)

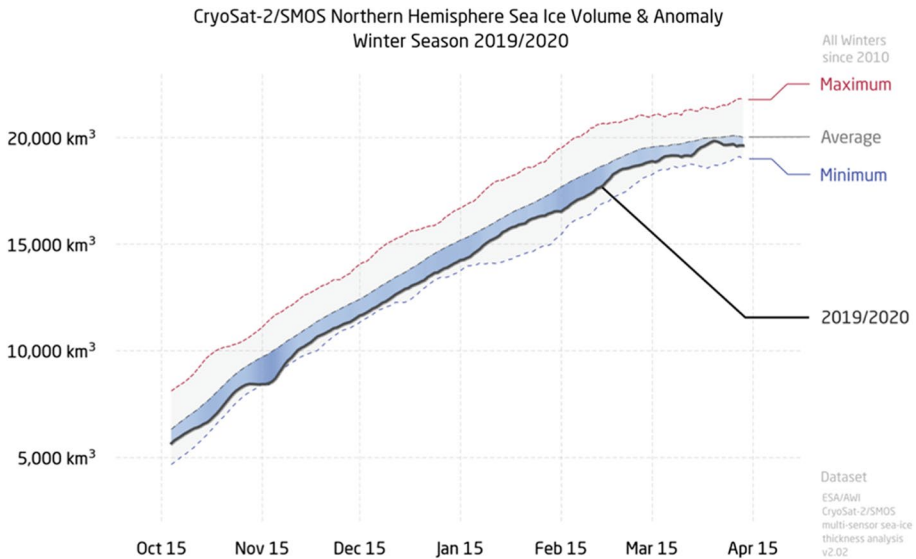


Fig. 9 Time series of Arctic sea ice volume in winter (spanning 15 October to 15 April) derived from the CryoSat-2/SMOS merged ice thickness product combined with passive microwave radiometer sea ice concentration data. Ice volume in winter 2019/20 (thick black line) is shown in the context of the 10-year climatology range (gray shading) for winter 2010/11 through winter 2019/20, bounded by the minimum (blue dashed line), maximum (red dashed line), and average (gray dot-dashed line) daily sea ice volumes for all winters since 2010. Reproduced from Perovich et al. (2020) (<https://doi.org/10.25923/n170-9h57>)

Analyzing the earliest thickness records from ERS-1/2, Laxon et al. (2003) found that the standard deviation of mean ice thickness over the first 8-year period of altimeter observations was 9% of the overall average ice thickness and moreover that average winter ice thickness was strongly correlated with the length of the summer melt season. Subsequent observations from ERS-1/2, Envisat, ICESat, CryoSat-2 and ICESat-2 have revealed a decline in Arctic sea ice thickness and volume over the last two decades (e.g., Perovich et al. 2020, Kwok and Cunningham 2015; Laxon et al. 2013; Giles et al. 2008a), during which time the sea ice cover has transitioned from a predominantly multi-year to seasonal ice pack (Druckenmiller et al. 2021). The greatest losses have been observed in areas containing the oldest and thickest sea ice (Figs. 8, 9). This transformation makes the Arctic ice cover more responsive to atmospheric conditions and more vulnerable to summer melt, thereby further amplifying the decline currently underway.

4.3 Snow Depth on Sea Ice

Due to the lack of atmospheric observations over the polar oceans, precipitation and snow accumulation on the pack ice remain poorly known. However, snow plays a very important role in the development of pack ice, thermal and gas exchanges, plankton growth and navigation. This snow also represents the first source of error in converting the freeboard measured by altimetry into ice thickness. Indeed, as can be seen in the conversion equations Eq. 4.1 and 4.2 of the previous section, both for the laser and the radar Ku measurements, the second term depends on the snow depth h_s . The density of snow being about 3 times lower than the density

of water, this second term in is about 2 times more important in the case of the laser f_s measurement (Eq. 4.1) than in the Ku f_i measurement (Eq. 4.2). On the other hand, the snow also induces an error on the f_i measurement because the propagation speed of Ku waves decreases in the snow, which leads to underestimate f_i . This underestimation can be corrected provided that the snow depth h_s is known. Thus, in the case of Ku radar, the snow depth is also included in the first term of the equation with an effect of about 25% of the snow depth.

It has been shown in Guerreiro et al. (2016) that using two radar frequencies, the Ku band with CryoSat-2 and the Ka band with the French-Canadian satellite Saral/AltiKa, one can measure the snow depth. Indeed, unlike the Ku frequency, which can penetrate several meters of snow (provided it is cold, dry and not salty), the Ka frequency is reflected close to the snow/air interface. Thus, the difference of the 2 heights Ka and Ku should provide the snow thickness. The main difficulty was coming from the footprint differences between CryoSat-2 and Saral, the first one being in SAR mode and the second in LRM mode, which aims to different impacts of the surface roughness on the range. The trick was to use CryoSat-2's LRM mode, a degraded SAR mode, which has a similar ground footprint to LRM. This allows the difference between Ka and Ku ranges to remove roughness effects. The DuST system presented in Lawrence et al. (2018) also estimates snow depth by Ka and Ku difference, but in this solution roughness effects are corrected by recalibration with Operation Ice Bridge airborne snow radar measurements (<https://icebridge.gsfc.nasa.gov/>).

Following the Guerreiro et al. (2016) methodology, Garnier et al. (2021) proposed the Alti Snow Depth (ASD) product over the Arctic and Southern Ocean sea ice covering the full Saral/AltiKa period (2013-present), as well as a monthly climatology that can reasonably be used from 2002 to cover the Envisat period. These studies have validated the methodology, which motivated the addition of a second frequency for the Copernicus CRISTAL polar altimeter project (see Sect. 8.3).

Several studies (Stroeve et al. 2020a, b and Nandan et al. 2017) showed that the penetration of the Ku-band in snow is limited by the presence of salt or moisture. It is therefore likely that these dual-frequency measurements underestimate the depth of the snow during fall ice formation, summer melt and in the marginal ice zone. The impact is probably even more important in the Southern Ocean due to frequent flooding effects and the presence of a slush layer. Work is ongoing to try to correct the measurements from these different effects according to other snow and ice parameters, such as the ice age and the surface temperatures.

Measuring snow depth by altimetry, as is planned with CRISTAL, will further increase the quality of the measurements for several essential reasons: (1) snow and freeboard measurements will be simultaneous, while because of the orbit differences between Saral and CryoSat-2 the current solutions calculate differences between monthly maps, (2) the sensor will be common for the 2 frequencies with similar footprints, (3) since the total freeboard f_s will be obtained by direct measurement with the Ka band, the uncertainty will be essentially in the position of the snow/ice transition: typically, an underestimation of snow will be partially compensated in terms of load by an overestimation of freeboard. In order to evaluate these types of effects, the orbit of CryoSat-2 was slightly modified in 2020 in the framework of the ESA Cryo2Ice project so that its trajectory periodically coincides with that of IceSat-2 and to perform synchronous Laser/Ku-band measurements.

5 Synthetic Aperture Radar

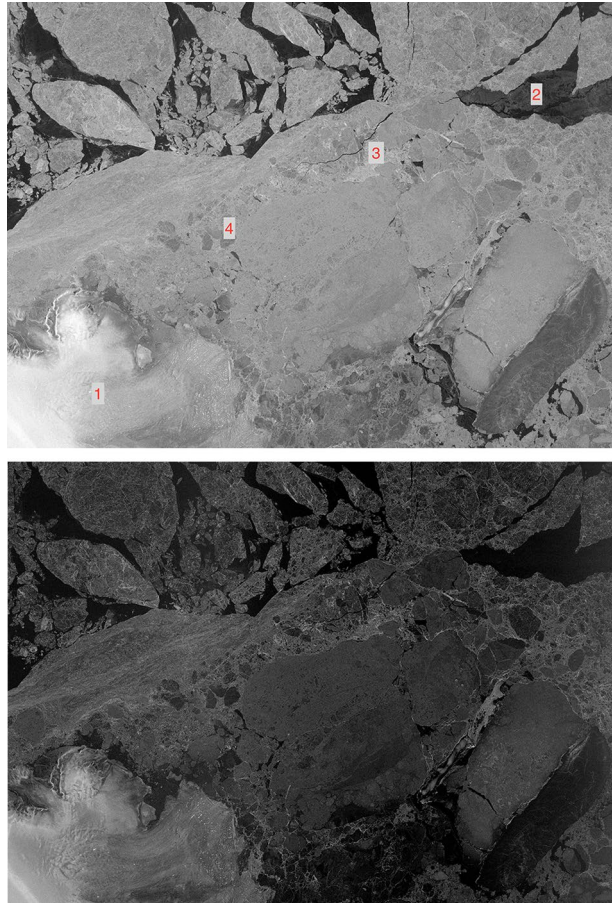
The synthetic aperture radar (SAR) is an imaging sensor operated on a number of Earth Observation satellites, starting with ERS-1 in 1991 and continuing with ERS-2, RADAR-SAT-1, ENVISAT and others. An overview of high-resolution imaging satellites including SAR is provided by, e.g., Elliot et al. (2016), (<https://www.nature.com/articles/ncomms13844/figures/2>). While passive microwave sensors and scatterometers operated on satellites provide spatial resolutions on the order of a few to many kilometers over swath widths between 500 and 1800 km, the corresponding numbers for satellite SAR systems are typically in the range of 1–100 m for the spatial resolution and between 10 and 500 km for the coverage in ground range direction. Both scatterometers and SAR sensors transmit and receive microwave radiation under oblique angles and hence measure the intensity that is scattered back to the sensor, while the nadir-looking altimeters receive the radar echoes directly reflected from the Earth's surface. Due to the difference in spatial resolution, the signals measured by scatterometers are usually mixtures of scattering contributions from different sea ice types, ice deformation zones, and open water areas located within one resolution cell, while the signals of spatially high-resolution cells typical for SAR systems often represent only a definite scattering mechanism from a homogenous ice area. Hence, SAR images can be used for assessments of data products obtained from coarse-resolution radiometer and scatterometer measurements and for complementing altimeter data, e.g., in separating ice and open water leads.

5.1 Operational Applications

Most important among the applications of SAR data is the operational production of *sea ice charts*, carried out at national ice services of which many are organized in the International Ice Charting Working Group (<https://nsidc.org/noaa/iicwg>). Ice charts show spatial variations of ice concentration, the position of the ice edge, and the regional and local distribution of different ice types, sometimes supplemented by information such as floe sizes or occurrence of icebergs. One distinguishes between *strategic information* which is useful for route planning at regional scales as provided in the daily ice charts, and *tactical information* which presents a detailed local analysis in the vicinity of a vessel or marine platform to support immediate operations. Strategic and tactical information is not only valuable for merchant ships and oil tankers on their passage through ice-covered waters in the far North or South, but, e.g., also for research vessels operating in the ice, and fishing vessels and cruise ships if they are moving close to the ice margin. Ice charts are usually updated daily or weekly but can also be produced on demand. Examples of ice charts can be found on the web sites of national ice services and of the Copernicus Marine Service (<https://marine.copernicus.eu>). As part of the Copernicus service, the following sea ice products are based on the analysis of SAR imagery, partly in combination with other sensors: arctic sea ice concentration; concentration, drift and thickness for the ice cover in the Baltic Sea; position of the ice edge in the Antarctic Ocean; iceberg concentration and individual iceberg positions along the coastal waters of Greenland, Newfoundland, and Labrador; and sea ice drift patterns in the Arctic. An example of HH and HV SAR images of sea ice northeast of Greenland is shown in Fig. 10.

Today, most ice charts are still manually generated by trained ice analysts, who by means of geographic information systems manipulate the available data such that they can

Fig. 10 Sentinel-1 images acquired at HH (upper image)- and HV (lower image)-polarization on 04 October 2021 over sea ice northeast of Greenland. The grey tone variations correspond to an interval of the backscattering coefficient between -27.5 and -2 dB. The width of the image is 115 km. Land ice is visible to the lower left (1). Stages of new ice formation (2) appear almost black at HV-polarization, whereas they can be distinguished at HH-polarization. The brightest zones (3) represent deformed ice (including brash ice between ice floes). The intensity contrast between deformed and level (4) ice is larger at HV-polarization in many areas. (From ESA Science Hub, processed with SNAP)



optimally interpret them in terms of ice conditions within short time, typically one hour. Besides SAR images acquired at like- and cross-polarization (usually HH, HV), images from optical satellite sensors, weather reports, and information from reconnaissance flights are used in addition, if available. An important attribute for interpretation is texture, i.e. local image brightness variations caused by structures on or in the ice. Such structures often provide a clue for separating ice types or identifying ice structures such as leads, shear zones, and pressure ridges. An example of an ice chart based on analysis of a SAR image is shown in Fig. 11.

A common practice in manual ice mapping is to include the temporal evolution of ice conditions. Also, data fusion between different types of sensors, the combination of SAR images acquired at different frequencies, and polarimetric data can be helpful. In case of polarimetric measurements, both amplitudes at different polarizations and phase differences between differently polarized signals are used for information retrieval. Considering the increasing number of operational satellite missions planned for the near future, a much larger number of images and complementary data will be available per day. This requires inclusion of semi- or fully automated processing strategies in ice charting. Here, key words are machine- and deep learning and artificial intelligence which are recently tested on SAR

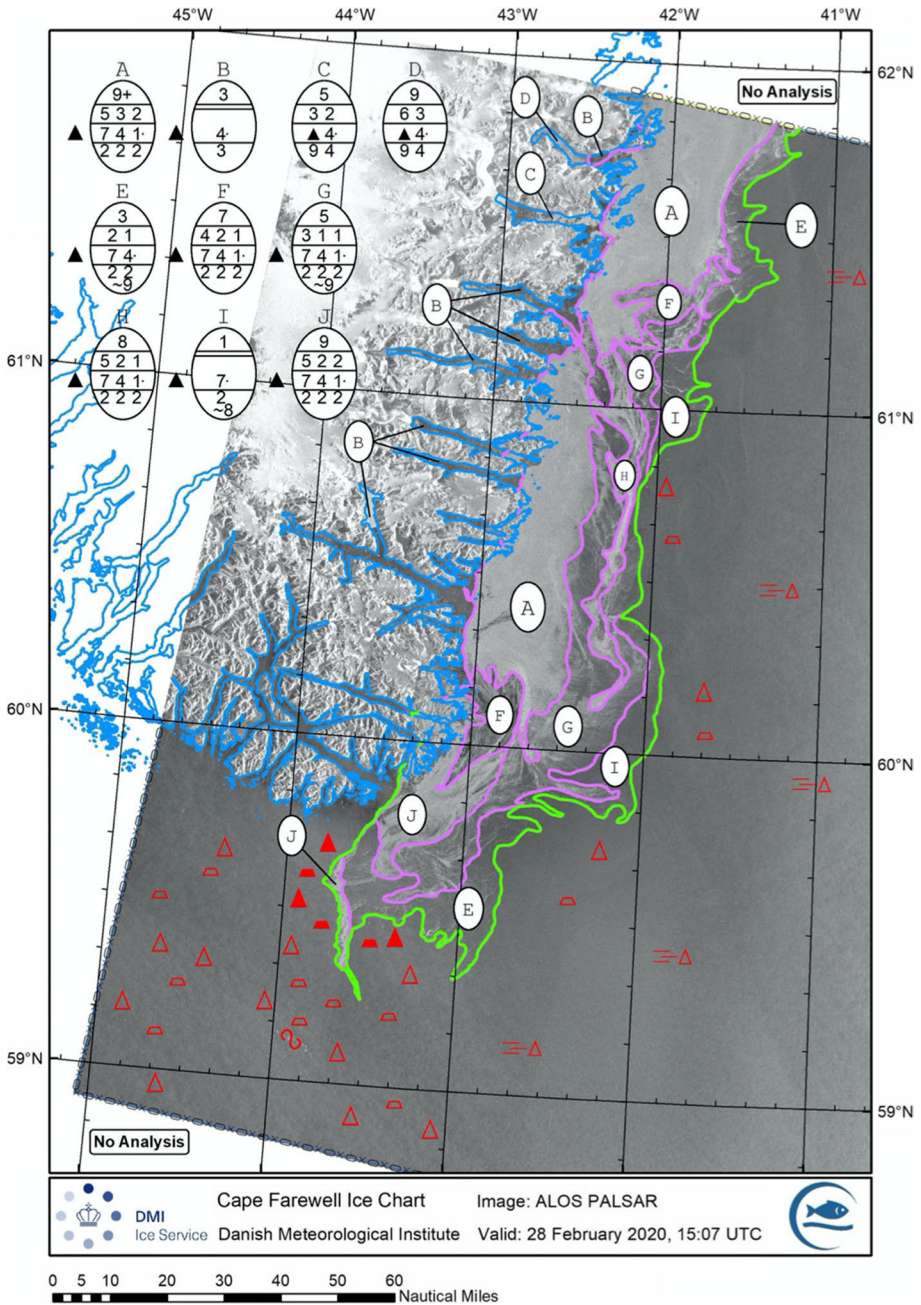


Fig. 11 PALSAR-2 WideBeam image acquired on 28 February 2020 with polygons separating ice areas with different characteristics, as inserted by an ice analyst from the Danish Meteorological Institute. The red data marks are used to indicate position of icebergs (red triangles) and growlers (red trapezoids). Open data marks symbolize few, filled marks many icebergs. Three parallel lines indicate ice free areas. The egg-shaped symbols contain information on total and partial ice concentrations, stage of development and form of the ice. (Courtesy of DMI)

images or on data from different sensors to find optimal combinations of frequencies, polarizations and complementary information for separating different ice types and for the retrieval of other ice parameters within short time. One distinguishes between supervised and unsupervised methods. The former requires training data which define the assignment of a set of image properties to a certain ice class. Unsupervised algorithms, which are run without training data, seek to identify image segments with similar statistical properties. The final—and challenging—step is then to label the different segments according to the classification scheme of the WMO. Different methods for automated ice charting and ice classification are introduced in Dierking (2020) and references cited therein.

5.2 Science Applications

The high-resolution data obtained from SAR systems are also exploited for developing a better understanding of the interaction between atmosphere, sea ice, and ocean, in particular focusing on local and regional sea ice processes, e.g., sea ice kinematics at spatial resolutions on the order of 100–1000 m, evolution of polynyas and leads, or growth, expansion, retreat and decay of the ice in the marginal ice zone. This helps to improve or validate numerical models for simulations of sea ice dynamics due to atmospheric and oceanic forcing. Such models are in turn relevant for parameterizations used in weather forecasts and climate models. SAR data also have contributed to applications typical for passive microwave radiometers, scatterometers, and altimeters (see sections above), but over smaller regions and with larger time gaps.

SAR image pairs and sequences are used to retrieve *sea ice displacement* vectors at spatial resolutions of tens to hundreds of meters over areas between a few tens and hundreds of kilometers, depending on the imaging mode and spatial overlap between the image pair. With single-satellite missions, however, temporal gaps between two images are mostly on the order of several hours and hence not sufficient to resolve, e.g., tidal effects. Temporal gaps can be reduced using, e.g., constellations of two or more identical SAR satellites with coordinated ground coverage, or different satellites which provide radar images with matching information over a given region. The most popular methods for the retrieval of motion from SAR images are pattern matching and feature tracking (e.g., Berg and Eriksson 2014; Korosov and Rampal 2017). Both methods rely on the presence of distinct and stable spatial radar intensity variation, caused, e.g., by the presence of ridges and ice floe edges. Pattern matching is based on correlation techniques, which may be coupled in pyramid-cascade approaches, starting at coarse spatial resolution which is refined step-by-step. Matching is hampered if ice deformation takes place between the acquisitions of image 1 and 2. In feature tracking, single distinct key elements, e.g. striking ice structures detected at different resolution levels, are identified by binary descriptors, or ice floe boundaries are translated to coordinate curves. The descriptors or curves are then compared between image 1 and image 2 to determine the position change of a given key element, usually accepting a small difference which is below a pre-defined threshold. While pattern matching provides drift vectors on regular grids, the key elements used in feature tracking are irregularly distributed over the image. The gradients of the displacement vectors can be used to calculate deformation parameters such as divergence/convergence or shear. Besides for science-driven questions, sea ice displacement retrievals start to be employed in assimilation into operational ice forecast models (Sect. 6).

The determination of sea ice displacement patterns and deformation is based on mature retrieval algorithms. Several studies for the retrieval of other ice parameters,

e.g., ice thickness, surface roughness, degree of deformation, timing of melt onset and freeze-up, and fast ice extent and stability, have been published, but their robustness and reliability is yet not sufficient for operational applications or general employment in scientific studies. A number of investigators noted correlations between *ice thickness* and radar backscattering coefficients at different polarizations or between thickness and the co-polarization ratio HH/VV, with a higher sensitivity to thickness changes for less thick ice (e.g., Wakabayashi et al. 2004). Other studies found correlations between the backscattering coefficient and *ice surface roughness* at horizontal scales between a few decimeters and meters. *Deformation* due to shear and compressive forces, which is recognized, e.g., as ice ridges and rafting zones, can be well detected in SAR images with spatial resolutions ≤ 10 m because of the higher backscattering intensity relative to the adjacent smooth level ice (Dierking and Dall 2007). An example of an ice drift map with estimated divergence/convergence is shown in Fig. 12.

While this is useful for evaluating ridge densities, first experiments with interferometric SAR (i.e. using the phase difference between two coherent SAR signals received at different sensor positions, where the distance between both is being called the interferometric baseline) showed a potential for the retrieval of ridge heights over fast or temporally stationary ice (Yitayew et al. 2018). For applications over drifting pack ice, however, this technique requires data from satellite tandems with very small temporal gaps between the received signals but sufficiently large baselines for achieving the required sensitivity to height variations. Interferometric SAR has also been used for mapping *fast ice extent* and the assessments of *fast ice stability* (Dammann et al. 2019). The *timing of melt-onset and freeze-up* is determined from significant changes in backscattering characteristics taking place within a few (1–4) days. These changes are caused by the reduction of the radar penetration depth when the ice surface starts to

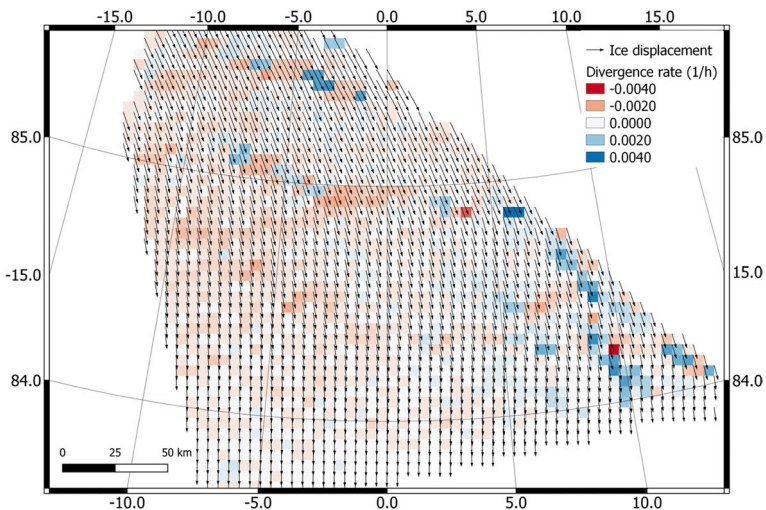


Fig. 12 Ice drift (arrows) and divergence (blue) /convergence (red) zones derived from an ALOS WB image (acquired 03 September 2019, 14:47 UTC) and a Sentinel 1 EW image (02 September 2019, 11:08 UTC). While ice drift is mostly retrieved from image pairs acquired at one frequency, the motivation of using L-C band pairs is (1) to increase the temporal sampling and (2) to use the drift for alignment of one image to the other as preparation for automated classification of L-C image pairs. (Courtesy of Chalmers / NERSC)

melt, and grain size and wetness of the snow cover on the ice increase (e.g., Casey et al. 2016).

5.3 Ice Parameter Retrieval

For retrieving information about ice properties, different SAR parameters have to be considered both in operational and science applications. These are mainly frequency, polarization, incidence angle, spatial resolution, and signal-to-noise ratio. The choice of the radar frequency determines the potential to separate different ice cover properties. For recent sea ice observations with satellite SAR, the frequencies mainly used are L-band (1–2 GHz), C-band (4–8 GHz), and X-band (8–12.5 GHz). Lower *frequencies* offer a more robust separation between deformed (e.g., ridged, rafted, brash) ice and smooth level ice and—due to their larger penetration depth—a better discrimination of certain ice types in some phases of the melting season. Higher frequencies on the other hand are in many cases well suited to distinguish multi-year, first-year, and new ice, but they are more sensitive to ice surface and snow properties on scales of a few millimeters to centimeters which may cause ambiguities in the interpretation of SAR images (see below). The separation of ice and open water is easier at HH- and cross (HV, VH)—*polarization* than at VV-polarization. Cross-polarization is also preferable for the identification of deformation zones. The *incidence angle* sensitivity of the backscattering coefficient differs between single ice types which requires to include it as an ice class property in automated classification of wide-swath SAR scenes that cover incidence angle ranges between 20° and more than 43° (Lohse et al. 2020). The *spatial resolution* determines which ice characteristics and structures are still recognizable for a robust ice classification. Finally, a high *noise level* makes it difficult or impossible to distinguish new ice types (e.g., nilas, grey ice) from one another and from smooth open water surfaces at low wind speeds because of their low backscattering intensity.

The identification of sea ice types and structure depends not only on the properties of the SAR system, but also on the relative influence of ice salinity, temperature, and millimeter to decimeter-scale ice properties. The latter are the small-scale surface roughness (on the order of the radar wavelength), brine cells, air bubbles, and the roughness of interfaces between different layers in the ice volume. The small-scale surface and interface roughness, together with the dielectric contrast between air (snow) and ice or between ice layers, determine the intensity of the surface and interface scattering. The contribution of volume scattering increases with decreasing salinity (i. e. lower brine content), provided that scattering elements (air bubbles, brine cells) are present in the ice. At temperatures slightly below or at 0 °C, the loss factor of the dielectric constant increases strongly, thus significantly reducing the penetration depth of radar signals into the ice. Snow cover properties (density, grain size) may affect the backscattered signal, too, depending on the radar frequency. If the snow is wet, the radar signal may even not penetrate down to the snow-ice interface. At low radar frequencies, the effect of snow on the backscattered signal is less. Since the small-scale ice properties do not differ consistently between different ice types and are dependent on weather conditions and season, their variations may cause ambiguities between radar signatures of different ice types. This is one fundamental reason for false ice classifications. For more information on SAR observations and monitoring of sea ice and icebergs, the reader is referred to the review article by Dierking (2013) and the

book chapter by Dierking (2020), in which also lists of references can be found which provide detailed descriptions of methods and results.

6 Modeling and Applications

Sea ice models are typically the sea ice component of coupled ice-ocean or fully-coupled atmosphere-ice-ocean modeling systems used to provide forecast guidance on ice thickness, ice concentration, ice strength, and ice drift at horizontal resolutions ranging from 2 to 10 km. The Community Ice CodE (CICE, Hunke and Lipscomb, 2008) and the Louvain-la-Neuve sea ice model (Roussel et al. 2015) are the most commonly used sea ice models by operational production centers with typical forecast lengths ranging from 5 to 10 days.

Ensemble-based systems consist of individual members ranging from 10 to 30+ members in which the initial state is perturbed in some manner such that the prediction varies for each member during the forecast period producing an *ensemble spread* to provide a sense of the possible variation in the end state. An example of this would be an ensemble prediction valid 30 days in the future providing a range in ice thickness for a particular location (grid point) of 1.4–1.8 m. In a similar fashion, the ice drift direction could indicate an ensemble spread of 45° at this same location at 30 days.

Most of these techniques are based on statistical approaches but it is important to mention the development of new sea ice modelling approaches that move towards explicitly representing the physical mechanisms that govern the dynamic processes within the ice pack (fracturing, faulting, damaging, damage healing, etc.). One can for example cite the development of a new class of rheologies (i.e. equation defining how stress and deformation relate to each other) that are adapted to a realistic simulation of the brittle nature of sea ice (Girard et al. 2011; Dansereau et al. 2016, Ólason et al. 2022). This new type of rheology has been only implemented in the finite element neXt Generation Sea Ice Model (neXtSIM, Rampal et al. 2016, 2019) so far, but some efforts are currently made to attempt its implementation in standard model based on finite difference like, e.g., SI3—the sea ice component of the NEMO ocean modelling platform (Hunke et al. 2020). The progress in the computing capacity, as well as the development of parallel versions of these numerical codes, have allowed operational centers to use sea ice models for providing real-time forecast over areas as large as the pan-Arctic region. Examples are TOPAZ (Sakov et al. 2012) and neXtSIM-F (Williams et al. 2021).

There are also a host of *climate* models which may also be part of a coupled modeling system, but typically have horizontal resolutions of 100's of km and may be run for periods of 50–100 years or longer. These models may be used in long-term hindcast studies for a number of reasons such as assessing the impact of climate change by examining the CO₂ levels in the atmosphere and the resulting change in Arctic sea cover. The Coupled Model Intercomparison Project Phase 6 (CMIP6, Eyring et al. 2016) encompasses a suite of such climate models in their studies. In some cases the climate models may be the same as used in operational production centers (Hunke et al. 2020), but at coarser resolutions.

Numerical forecast models require initialization to provide the best possible initial conditions prior to generating a forecast. Sea ice models are usually spun-up over a period of several years until an equilibrium state is reached. Prior to producing a sea ice forecast, satellite-derived ice concentration is used to specify regions of complete ice cover (100% ice concentration) to open water (0% ice concentration). In a coupled system, satellite-derived sea surface temperatures are used to initialize the sea surface temperature. Most

coupled modeling systems assimilate observational data (Smith et al. 2019) into the atmosphere (e.g., surface observations and upper-air soundings), ocean (sea surface temperature, ocean profile data, altimeter height etc.), and sea ice (ice concentration, sea ice thickness or freeboard) components. The assimilation of the thickness of the ice pack is more recent. Indeed, it was necessary to wait for the progress of SAR altimetry to obtain a better confidence on these measurements (see Sect. 4). Various studies have shown that assimilation of these data can increase forecasts from a few days to a few months (Blockley and Peterson 2018, Allard et al. 2018; Xie et al. 2018; Fiedler et al. 2022). Indeed, the fate of the pack ice at these time scales is essentially related to its thickness and its ability to withstand climatic hazards such as heat waves and gales.

Sea ice models (Smith et al. 2019) and available imagery are used by analysts at the Canadian Ice Service (CIS) and US National Ice Center (NIC) for vessel routing and to provide guidance to icebreakers which have the ability to transit through ice up to several meters thick. These analysts also provide information on where to expect sea ice, so ships and vessels can avoid the ice. In addition, both the CIS and NIC provide forecasts of iceberg trajectories in the northern Atlantic waters. NOAA's Great Lakes Environmental Research Laboratory provides seasonal ice forecasts and charts for the Great Lakes. Sea ice forecasts are generated by ECMWF and several national ice centers. These forecasts are also used to support field campaigns in ice-covered regions.

The biannual Ice Experiment (ICEX) occurs in even years (e.g., 2018, 2020, 2022) in the Beaufort Sea. Analysts at the NIC in conjunction with the Arctic Submarine Laboratory examine imagery several weeks prior to ICEX to determine potential ice floes in which an ice camp will be established for the late February/March time period. The ice floe must be comprised of multi-year ice to support landing of aircraft to provide supplies needed to establish and maintain the ice camp. In addition, low-flying aircraft may be used in making the final determination on the ideal floe. Lastly, in case of evacuation of the ice camp due to significant fractures or leads impacting the ice camp, the ice floe must be within a particular distance from aircraft landing sites in Alaska. Once the ice camp is established, the crew will reside on the ice flow and perform experiments on the ice for up to a 30-day period. Figure 13 depicts a 4-day forecast of the ice strain and fracturing rate

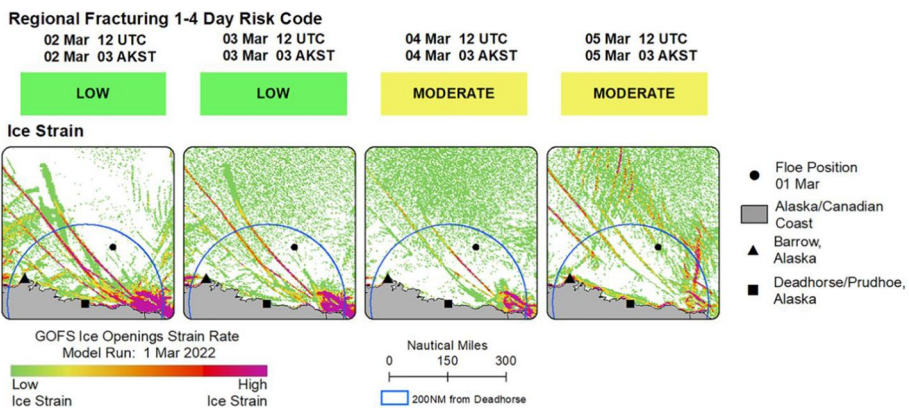


Fig. 13 NIC ICEX 2018 support product depicting a 5-day forecast of ice fracturing risk based on lead opening rate in the CICE model. (Image courtesy of USNIC)

based on CICE (Hunke and Lipscomb 2008, Hunke et al. 2020) model output. The graphic is used for guidance in support of ICES with the ice floe depicted as a black circle.

Another example of the use of ice forecasting products is the annual McMurdo Resupply mission which occurs in the Ross Sea (Antarctic) every February. The US Coast Guard’s

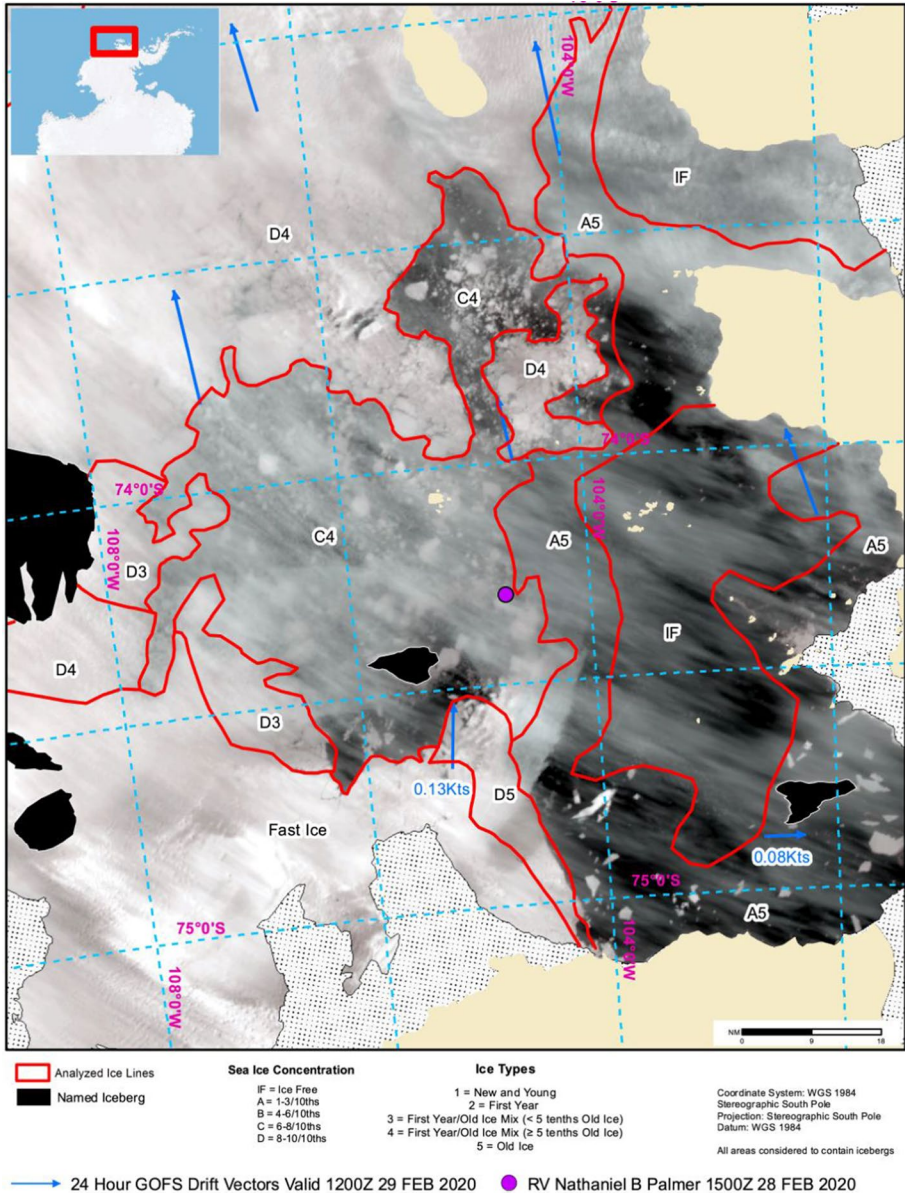


Fig. 14 USNIC support graphic depicting location of the R/V Nathaniel B. Palmer (purple circle), ice coverage (tenths) in the Amundsen Sea, and CICE ice drift vectors (blue arrows) on 20 February 2020. (Image courtesy of USNIC)

heavy icebreaker *Polar Star* is used to cut through the ice so resupply ships can safely reach McMurdo Station on Ross Island in the Ross Sea where the National Science Foundation operates a 154-acre research facility. The NIC (which produces forecast products for the Arctic and Antarctic) supports this mission providing daily forecast guidance. The NIC provided support to the *R/V Nathaniel Palmer* in the Amundsen Sea in February 2020 as part of the NSF International Thwaites Glacier Collaboration. The research vessel had difficulty identifying an exit location from the ice. The NIC provided forecast support as shown in Fig. 14 which depicts CICE ice drift vectors overlaid on imagery. The *R/V Nathaniel Palmer* was successful using the NIC products to navigate out of the ice-laden waters.

Sea ice models predictions are used to support the Sea Ice Prediction Network (SIPN2) in which contributors are invited to generate a 5-month prediction (initialized May 1) of the September Arctic minimum extent. Submissions (<https://www.arcus.org/sipn/sea-ice-outlook/2021/september>) are based on dynamical models, heuristic or qualitative analyses, statistical methods, and machine learning. Figure 15 shows the range in prediction of the September 2021 sea ice extent using all these techniques. The actual observed minimum of 4.72 million km² (solid black vertical line) was reached on 16 September, 2021. This process is repeated with 01 June (4-month prediction) and 01 July (3-month prediction) initialization.

Sea ice models have also been used to provide daily forecasts in the Multidisciplinary drifting Observatory for the Study of Arctic Climate (MOSAiC), in which the *R/V Polarstern* icebreaker was frozen into the ice from Fall 2019 to early Summer 2020. Starting off the coast of Norway in September, 2019 the MOSAiC team collected in situ observations in the Arctic to help understand coupled climate processes in the Central Arctic.

The Sea Ice Drift Forecast Experiment (SIDFEX) is a community effort to collect and analyse Arctic sea ice drift forecasts at lead times from days to up to a year, for a number of

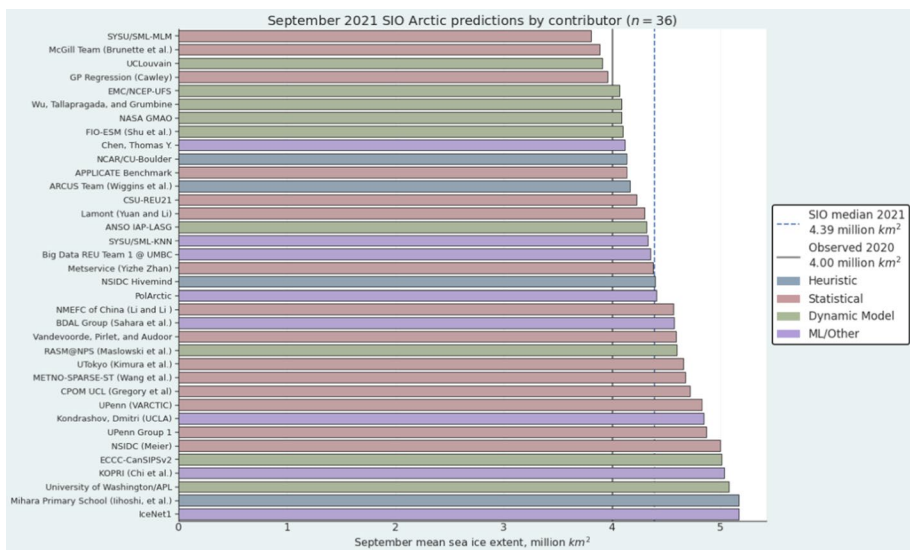


Fig. 15 SIPN2 forecast (initialized 01 May 2021) from 38 contributions of Arctic September minimum sea ice extent (million km²). Actual observed extent of 4.72 million km² observed on 16 September 2021. (<https://www.arcus.org/sipn/project-team>)

sea-ice buoys on a regular basis. Drift trajectories at a number of Arctic locations provide valuable insight on how the sea ice models perform in different Arctic regions and seasons.

In the wake of increasing amounts of satellite data available for sea ice observation, services are evolving to provide tailor-made products to the user groups, including ice navigation (Wagner et al. 2020). The services are mostly provided by national weather and ice services which also provide forecasting. On international level the Copernicus Marine Environmental services (CMEMS) delivers a portfolio of sea ice monitoring (<https://marine.copernicus.eu/about/producers/seaice-tac>) and forecasting products (<https://www.nersc.no/project/arc-mfc>).

7 Support to Ice Navigation

Navigation of icebreakers in the polar seas and other ice-covered sailing routes is an important application of satellite data, using data from most of the sensors providing regular coverage of the sea ice areas. Ice navigation has a long history in regions such as the Baltic Sea, the Canadian Arctic, Eastern Canada, St. Lawrence Seaway, around Greenland and Svalbard, and the Northern Sea Route (Johannessen et al. 2007). Use of satellite data to map sea ice in support of ship traffic has developed since the 1970s, following many decades of airborne surveys.

The use of optical and infrared images from Sun-synchronous polar orbiting satellites started in the 1970s and have continued as one of the data sources to support ice navigation. The usefulness of these data is limited by cloud-cover and darkness. The use of passive microwave data, starting also in the 1970s, have been the backbone of operational ice charting because of the regularity of data provision, independent of weather and light conditions. The usefulness of these data for ice navigation is enhanced when the data are downloaded, analysed and transmitted to the vessel in near-real time. The limitation of the passive microwave data is mainly the coarse resolution, implying that ice characteristics on scales less than a few km are not captured.

The advancement of Synthetic Aperture Radars represented a milestone in mapping sea ice because the high resolution of the images provides detailed information about leads, ice types and other ice characteristic of importance for ice navigation. SAR systems were first operated on aircraft in the 1980s and from the 1990s several satellite SAR systems have been in operations. In fact, ice navigation has been one of the drivers for SAR satellites and delivery of data in near realtime to users. In particular the RADARSAT and the ERS/ENVISAT programs were instrumental in developing SAR-based ice monitoring to support ice navigation. From 2014 the Sentinel-1 satellites have extended to provision of SAR data significantly, by delivering regular coverage of the shipping lanes in the Arctic. The interval of the images is from 1 to 3 days with dissemination to users within a few hours. The capability to deliver repeated SAR images in the same areas provide valuable information about the dynamics of the sea ice in particular ice motion, leads, ridges, rough ice areas, fastice, large floes, etc. However, the requirements for timely ice information will depend on the type of vessel and the ice conditions along the sailing routes. Large and powerful icebreakers are less dependent on detailed ice information, while smaller ice-strengthened vessels need more specific information about thick ice ridges and other ice obstacles. During mooring deployment, seafloor drilling or other operations in sea ice there are other more strict requirements for observational data where satellite data is only a part of the total observing system. A particular limitation of the satellite data is the temporal

coverage, where polar orbiting satellites at best provide data twice per day. The operations need continuous ice monitoring, which requires use of ship radar, drones, helicopters and drifting ice buoys, all of which transmit realtime data to the operational headquarters.

Full benefit of the SAR data in ice navigation is difficult because data transmission to ships in the Arctic is limited. A SAR image is typically 200–300 Mbyte which can take hours to transmit using Iridium. It is therefore not feasible to transmit a several images per day with the present communication services in the Arctic. This will improve when satellite broadband services become available within a few years. Shipping activities in the Arctic is expected to grow in the coming years due to increased tourism, oil and gas exploitation in Russia, and the interest from many countries to explore mineral and other resources in the Arctic.

8 Conclusions and Future Outlook

8.1 The Future of Microwave Radiometer Sea Ice Observations

Currently, the main source for daily global sea ice concentration is AMSR2 on GCOM-W. The satellite has been in orbit since 2012 and is fully operational, exceeding its nominal life time of 5 years. The successor AMSR3 is scheduled for launch in 2024, hoping that the climatological time series of geophysical parameters based on passive microwave sensor observations will be continued without interruption.

To improve the spatial resolution of sea ice parameters and reduce their uncertainty is the goal of the upcoming Copernicus Imaging Microwave Radiometer (CIMR), one of the six Copernicus Sentinel Expansion missions. Its antenna reflector of 8 m diameter will allow daily sea ice concentration retrievals of better than 5 km resolution with lower uncertainty (Kilic et al. 2018) and many additional sea ice parameters like ice type, ice temperature and thin ice thickness (Scarlat et al. 2020). As the observations are done in the range from 1.4 to 36.5 GHz, the uncertainty caused by atmospheric influence will be much lower than, for example, in the 89 GHz ASI retrievals (Sect. 2.1). Also, sea ice motion and snow on sea ice will be retrieved at higher spatial resolutions than today. Moreover, based on the L-band passive microwave data from CIMR, the time series of thin ice thickness from SMOS and SMAP will be continued.

8.2 Perspective on Scatterometry

Scatterometers have proven they are useful for sea ice monitoring, although, multi-missions multi-resolution synergy between low scale scatterometer and high resolution would be helpful for sea ice drift estimate in coastal polar areas including the Baltic Sea. Moreover, microwave are sensitive to melting at the surface and summer observations remain poorly evaluated. The ice extent, displacement and type can be inferred from scatterometers onboard satellites, several methods exist and the continuity of C and Ku-band scatterometer would be helpful to continue the long-term monitoring of polar areas in addition to the use of tandem of sensors to have a full polar coverage at daily scale such as ASCATs onboard MetOp-A & B.

8.3 Perspective on Altimetry

Given societal needs for accurate sea ice thickness observations for both operational activities in ice-infested waters and to understand and predict the impacts of Earth's changing climate system, ongoing monitoring of Arctic and Southern Ocean sea ice thickness with satellite altimetry is required. Indeed, a continuous time series is necessary to determine if recent observations are part of a sustained negative trend or a reflection of natural, inter-annual variability in the polar climate. The Copernicus polaR Ice and Snow Topography Altimeter (CRISTAL) mission is currently being developed as part of the European Copernicus Program of Sentinel-series satellite missions. The mission comprises 2 satellites with an orbit optimized for monitoring the polar regions and a Ku/Ka dual-band SAR altimeter to measure sea ice and land ice elevation (Kern et al. 2020). Thanks to these 2 frequencies, we will be able to measure for the first time the freeboard of the pack ice and the snow depth simultaneously. Thus we will be able to determine in real time the thickness of the ice pack.

One of the primary goals of the mission is to provide continuity in observations of the topography of the polar oceans and their ice cover, and it therefore has a 7.5 years design lifetime and high along-track resolution to distinguish open ocean from sea ice surfaces. The mission should be launched in 2027 and is expected to contribute to the long-term altimetry record of Arctic and Southern Ocean sea ice freeboard, thickness and volume. CRISTAL is currently the only satellite altimeter proposed for near-complete polar observation and is therefore the only option for continuity of the unique geographical coverage currently obtained by CryoSat-2 and ICESat-2 over the Arctic Ocean as well as the Antarctic Polar Cap. It is therefore considered by the sea ice community to be a high priority mission, since it is the only mechanism for sustained monitoring of changes in the thickest multi-year sea ice found north of 81.5°N in the Arctic Ocean.

8.4 Synthetic Aperture Radar—New strategies

To overcome drawbacks of former or of some recent satellite mission, the following mission strategies have been or will be implemented besides many sensor improvements: constellations of two or more SAR satellites to increase the revisit rate and coverage (e.g., Sentinel 1A and 1B, Radarsat Constellation Mission of three identical C-band and COSMO SkyMed of four X-band SAR satellites); wide-coverage SAR image modes with higher spatial resolution for the detection of smaller objects and narrow ice structures (e.g., Sentinel 1 Next Generation); coordinated data acquisitions with SAR systems of different frequencies (L and C: ESA's ROSE-L with Sentinel-1 and Sentinel 1 Next Generation; L and X: Argentinian SAOCOM and Italian COSMO SkyMed), compact polarimetric (CP) and fully polarimetric (QP) modes (e.g., CP: Radarsat Constellation Mission, QP: Radarsat-2, Sentinel-1 NG), and both the multi-frequency and the polarimetric missions for increasing classification and retrieval accuracies. Furthermore, the development of new algorithms for multi-sensor, multi-mode ice classification by means of, e.g., different types of Neural Networks (deep learning) or information theory is an essential component for increasing the robustness and reliability of ice charts and parameter retrievals from SAR and complementary sensors.

Funding This research has been partly supported by the European Union's Horizon 2020 research and innovation programme via projects INTAROS (INTEgrated Arctic Observation System; Grant No. 727890) and CRiceS (Climate Relevant interactions and feedbacks: the key role of sea ice and Snow in the polar and global climate system; Grant No. 101003826). W. Dierking's contribution was partly funded by CIRFA

partners and the Research Council of Norway (RCN) (Grant No. 237906). The authors have no relevant financial or non-financial interests to disclose.

Declarations

Conflict of interest All authors declare that they have no conflict of interest.

Human and Animal Rights The article does not contain any studies with human participants or animals performed by any of the authors.

Open Access This article is licensed under a Creative Commons Attribution 4.0 International License, which permits use, sharing, adaptation, distribution and reproduction in any medium or format, as long as you give appropriate credit to the original author(s) and the source, provide a link to the Creative Commons licence, and indicate if changes were made. The images or other third party material in this article are included in the article's Creative Commons licence, unless indicated otherwise in a credit line to the material. If material is not included in the article's Creative Commons licence and your intended use is not permitted by statutory regulation or exceeds the permitted use, you will need to obtain permission directly from the copyright holder. To view a copy of this licence, visit <http://creativecommons.org/licenses/by/4.0/>.

References

- Allard RA, Farrell SL, Hebert DA, Johnston WF, Li L, Kurtz NT, Phelps MW, Posey PG, Tilling R, Ridout A, Wallcraft AJ (2018) Utilizing CryoSat-2 sea ice thickness to initialize a coupled ice-ocean modeling system. *Adv Space Res the CryoSat Satell Altimetry Miss Eight Years Sci Exploit* 62:1265–1280. <https://doi.org/10.1016/j.asr.2017.12.030>
- Barry R, Gan TY (2011) *The global cryosphere: past present and future*. Cambridge University Press, Cambridge, pp 489
- Belmonte-Rivas M, Otosaka I, Stoffelen A, Verhoef A (2018) A scatterometer record of sea ice extents and backscatter: 1992–2016. *Cryosphere* 12:2941–2953. <https://doi.org/10.5194/tc-12-2941-2018>
- Berg A, Eriksson LEB (2014) Investigations of a hybrid algorithm for sea ice drift measurements using synthetic aperture radar images. *IEEE Trans Geosci Remote Sens* 52(8):5023–5033. <https://doi.org/10.1109/TGRS.2013.2286500>
- Bi H, Zhang Z, Wang Y, Xu X, Liang Y, Huang J, Liu Y, Fu M (2019) Baffin Bay sea ice inflow and outflow : 1978–1979 to 2016–2017. *Cryosph* 13:1025–1042. <https://doi.org/10.5194/tc-13-1025-2019>
- Blockley EW, Peterson KA (2018) Improving Met Office seasonal predictions of Arctic sea ice using assimilation of CryoSat-2 thickness. *Cryosph* 12:3419–3438. <https://doi.org/10.5194/tc-12-3419-2018>
- Bocquet M, Fleury S, Piras F, Rinne E, Sallila H, Garnier F, Rémy F (2022) Arctic sea ice radar freeboard retrieval from ERS-2 using altimetry: Toward sea ice thickness observation from 1995 to 2021. Submitted in *The Cryosphere, reference egosphere-2022–214*
- Casey JA, Howell SEL, Tivy A, Haas C (2016) Separability of sea ice types from wide-swath C- and L-band synthetic aperture radar imagery acquired during the melt season. *Remote Sens Environ* 174:314–328. <https://doi.org/10.1016/j.rse.2015.12.021>
- Cavaliere DJ, Gloersen P, Campbell WJ (1984) Determination of sea ice parameters with the NIMBUS-7 SMMR. *J Geophys Res* 89(ND4):5355–5369
- Dammann DO, Eriksson LEB, Mahoney AR, Eicken H, Meyer FJ (2019) Mapping pan-Arctic landfast sea ice stability using Sentinel-1 interferometry. *Cryosphere* 13:557–577. <https://doi.org/10.5194/tc-13-557-2019>
- Dansereau V, Weiss J, Saramito P, Lattes P (2016) A Maxwell elasto-brittle rheology for sea ice modelling. *Cryosphere* 10:1339–1359. <https://doi.org/10.5194/tc-10-1339-2016>
- Dierking W (2013) Sea ice monitoring by synthetic aperture radar. *Oceanography* 26(2):100–111. <https://doi.org/10.5670/oceanog.2013.33>
- Dierking W, Dall J (2007) Sea ice deformation state from synthetic aperture radar imagery - part 1: comparison of C- and L-band and different polarizations. *IEEE Trans Geosci Remote Sens* 45(11):3610–3622. <https://doi.org/10.1109/TGRS.2007.903711>
- Dierking W (2020): Sea ice and Icebergs. In: G. Di Martino and A. Iodice (eds), *Maritime surveillance with synthetic aperture radar*, Institution of Engineering and Technology, vol 346 pp.173–225. <https://doi.org/10.1049/SBRA521E>

- Druckenmiller ML, Moon T, Thoman R (2021) The Arctic [in “State of the Climate in 2020”]. *Bull Amer Meteor Soc* 102(8):S263–S315. <https://doi.org/10.1175/BAMS-D-21-0086.1>
- Elliott J, Walters R, Wright T (2016) The role of space-based observation in understanding and responding to active tectonics and earthquakes. *Nat Commun* 7:13844. <https://doi.org/10.1038/ncomms13844>
- Emery WJ, Fowler CW, Maslanik JA (1997) Satellite-derived maps of Arctic and Antarctic sea ice motion: 1988 to 1994. *Geophys Res Lett*. <https://doi.org/10.1029/97GL00755>
- Eyring V, Bony S, Meehl GA, Senior CA, Stevens B, Stouffer RJ, Taylor KE (2016) Overview of the coupled model intercomparison project phase 6 (CMIP6) experimental design and organization. *Geosci Model Dev* 9:1937–1958. <https://doi.org/10.5194/gmd-9-1937-2016>
- Farrell SL, Laxon SW, McAdoo DC, Yi D, Zwally J (2009) Five years of Arctic sea ice freeboard measurements from the Ice, Cloud and land Elevation Satellite. *J Geophys Res Oceans* 114(C4):C04008
- Farrell SL et al (2011) A first assessment of IceBridge snow and ice thickness data over Arctic sea ice. *IEEE Trans Geosci Remote Sens* 50(6):2098–2111
- Fiedler EK, Martin MJ, Blockley E, Mignac D, Fournier N, Ridout A, Shepherd A, Tilling R (2022) Assimilation of sea ice thickness derived from CryoSat-2 along-track freeboard measurements into the Met Office’s Forecast Ocean Assimilation Model (FOAM). *Cryosphere* 16:61–85. <https://doi.org/10.5194/tc-16-61-2022>
- Garnier F, Fleury S, Garric G, Bouffard J, Tsamados M, Laforge A, Boucquet M, Hansen RMF, Remy F (2021) Advances in altimetric snow depth estimates using bi-frequency SARAL and CryoSat-2 Ka–Ku measurements. *Cryosphere* 15(12):5483–5512
- GCOS (2016) GCOS-200: The global observing system for climate: implementation needs. https://library.wmo.int/doc_num.php?explnum_id=3417
- Giles KA, Laxon SW, Wingham DJ, Wallis DW, Krabill WB, Leuschen CJ, McAdoo D, Manizade SS, Raney RK (2007) Combined airborne laser and radar altimeter measurements over the Fram Strait in May 2002. *Remote Sens. Environ* 111:182–194
- Giles KA, Laxon SW, Ridout AL (2008a) Circumpolar thinning of Arctic sea ice following the 2007 record ice extent minimum. *Geophys Res Lett* 35:L22502. <https://doi.org/10.1029/2008GL035710>
- Giles KA, Laxon SW, Worby AP (2008b) Arctic sea ice elevation from satellite radar altimetry. *Geophys Res Lett* 35:L03503. <https://doi.org/10.1029/2007GL031572>
- Girard L, Bouillon S, Weiss J, Amirano D, Fichet T, Legat V (2011) A new modeling framework for sea-ice mechanics based on elasto-brittle rheology. *Ann Glaciol* 52(57):123–132. <https://doi.org/10.3189/172756411795931499>
- Girard-Ardhuin F, Ezraty R (2012) Enhanced Arctic sea ice drift estimation merging radiometer and scatterometer data. *IEEE Trans Geosci Remote Sens* 50(7):2639–2648. <https://doi.org/10.1109/TGRS.2012.2184124>
- Guerreiro K, Fleury S, Zakharova E, Rémy F, Kouraev A (2016) Potential for estimation of snow depth on Arctic sea ice from CryoSat-2 and SARAL/AltiKa missions, *Remote Sens. Environ* 186:339–349
- Guerreiro K, Fleury S, Zakharova E, Kouraev A, Rémy F, Maisongrande P (2017) Comparison of CryoSat-2 and ENVISAT radar freeboard over Arctic sea ice: toward an improved Envisat freeboard retrieval. *Cryosphere* 11:2059–2073. <https://doi.org/10.5194/tc-11-2059-2017>
- Hendricks S, Paul S, Rinne E (2018) ESA Sea Ice Climate Change Initiative (Sea_Ice_cci): Northern hemisphere sea ice thickness from the Envisat satellite on a monthly grid (L3C), v2.0. Centre Environ Data Anal. <https://doi.org/10.5285/f4c34f4f0f1d4d0da06d771f6972f180>
- Hendricks S, Ricker R, Helm V (2016) User guide—AWI CryoSat-2 sea ice thickness data product (v1.2). <https://doi.org/hdl:10013/epic.48201>
- Hunke E, Lipscomb W (2008) CICE: the los alamos sea ice model documentation and software user’s manual Version 4.0. Tech. Rep. LA-CC-06–012. Los Alamos Natl Lab, Los Alamos
- Hunke E, Allard R, Blain P et al (2020) Should sea-ice modeling tools designed for climate research be used for short-term forecasting? *Curr Clim Change Rep* 6:121–136. <https://doi.org/10.1007/s40641-020-00162-y>
- Huntemann M, Heygster G, Kaleschke L, Krumpen T, Mäkynen M, Drusch M (2014) Empirical sea ice thickness retrieval during the freeze-up period from SMOS high incident angle observations. *Cryosphere* 8:439–451. <https://doi.org/10.5194/tc-8-439-2014>
- International Altimetry Team (2021) Altimetry for the future: Building on 25 years of progress. *Adv Space Res*. <https://doi.org/10.1016/j.asr.2021.01.022>
- IPCC (2021): Climate Change 2021: The Physical Science Basis. Contribution of Working Group I to the Sixth Assessment Report of the Intergovernmental Panel on Climate Change In: Masson-Delmotte, V., P. Zhai, A. Pirani, S.L. Connors, C. Péan, S. Berger, N. Caud, Y. Chen, L. Goldfarb, M.I. Gomis, M. Huang, K. Leitzell, E. Lonnoy, J.B.R. Matthews, T.K. Maycock, T. Waterfield, O.

- Yelekcı, R. Yu, and B. Zhou (eds.) Cambridge University Press, Cambridge, United Kingdom and New York, NY, p 2391 <https://doi.org/10.1017/9781009157896>
- Itkin P, Spreen G, Cheng B, Doble M, Girard-Ardhuin F, Haapala J, Hughes N, Kaleschke L, Nicolaus M, Wilkinson J (2017) Thin ice and storms : a case deformation from buoy arrays deployed during N-ICE2015. *J Geophys Res Ocean* 122:4661–4674. <https://doi.org/10.1002/2016JC012403>
- Ivanova N, Pedersen LT, Tonboe RT, Kern S, Heygster G, Lavergne T, Sørensen A, Saldo R, Dybkjær G, Brucker L, Shokr M (2015) Inter-comparison and evaluation of sea ice algorithms: towards further identification of challenges and optimal approach using passive microwave observations. *Cryosphere* 9:1797–1817
- Johannessen OM, Alexandrov VYu, Frolov V, Sandven S, Miles M, Pettersson LH, Bobylev LP, Kloster K, Smirnov VG, Mironov EU, Babich NG (2007) Polar Seas oceanography, remote sensing of sea ice in the Northern sea route: studies and applications. Springer, Berlin, p 472. <https://doi.org/10.1007/978-3-540-48840-8>
- Johannessen OM, Bobylev LP, Shalina EV, Sandven S (2020) Sea ice in the Arctic – past, present and future. Springer, Berlin, p 575. <https://doi.org/10.1007/978-3-030-21301-5>
- Kern S, Ozsoy-Cicek B, Willmes S, Nicolaus M, Haas C, Ackley S (2011) An intercomparison between AMSR-E snow-depth and satellite C- and Ku-band radar backscatter data for Antarctic sea ice. *Ann Glaciol* 52:279–290
- Kern M, Cullen R, Berruti B, Bouffard J, Casal T, Drinkwater MR, Gabriele A, Lecuyot A, Ludwig M, Midthassel R, Navas Traver I, Parrinello T, Ressler G, Andersson E, Martin Puig C, Andersen O, Bartsch A, Farrell SL, Fleury S, Gascoïn S, Guillot A, Humbert A, Rinne E, Shepherd A, van den Broeke MR, Yackel J (2020) The copernicus polar ice and snow topography altimeter (CRISTAL) high-priority candidate mission. *Cryosphere* 14:2235–2251. <https://doi.org/10.5194/tc-14-2235-2020>
- Kilic L, Prigent C, Aires F, Boutin J, Heygster G, Tonboe RT, Roquet H, Jimenez DC (2018) Expected performances of the copernicus imaging microwave radiometer (CIMR) for an all-weather and high spatial resolution estimation of ocean and sea ice parameters. *J Geophys Res Oceans* 123(10):7564–7580. <https://doi.org/10.1029/2018JC014408>
- Korosov AA, Rampal P (2017) A combination of feature tracking and pattern matching with optimal parametrization for sea ice drift retrieval from SAR data. *Remote Sens* 9:258. <https://doi.org/10.3390/rs9030258>
- Kruppen T, von Albedyll L, Goessling HF, Hendricks S, Juhls B, Spreen G, Willmes S, Belter HJ, Dethloff K, Haas C, Kaleschke L, Katlein C, Tian-Kunze X, Ricker R, Rostosky P, Rückert J, Singha S, Sokolova J (2021) MOSAiC drift expedition from October 2019 to July 2020: Sea ice conditions from space and comparison with previous years. *Cryosphere* 15:3897–3920. <https://doi.org/10.5194/tc-15-3897-2021>
- Kwok R, Cunningham GF (2015) Variability of Arctic sea ice thickness and volume from CryoSat-2. *Phil Trans R Soc A* 373(2045):20140157
- Kwok R, Zwally HJ, Yi (2004) ICESat observations of Arctic sea ice: a first look. *Geophys Res Lett* 31(16):L16401
- Kwok R, Kacimi S, Webster M, Kurtz N, Petty A (2020) Arctic snow depth and sea ice thickness from ICESat-2 and CryoSat-2 freeboards: a first examination. *J Geophys Res Oceans* 125:e2019JC016008
- Lavergne T, Eastwood S, Tefah Z, Schyberg H, Breivik LA (2010) Sea ice motion from low-resolution satellite sensors: An alternative method and its validation in the Arctic. *J Geophys Res* 115:C10032
- Lavergne T, Sørensen AM, Kern S, Tonboe RT, Notz D, Aaboe S, Bell L, Dybkjær G, Eastwood S, Gabarro C, Heygster G, Killie MA, Brandt Kreiner M, Lavelle J, Saldo R, Sandven S, Pedersen LT (2019) Version 2 of the EUMETSAT OSI SAF and ESA CCI sea-ice concentration climate data records. *Cryosphere* 13:49–78. <https://doi.org/10.5194/tc-13-49-2019>
- Lawrence IR, Tsamado MC, Stroeve JC, Armitage TWK, Ridout AL (2018) Estimating snow depth over Arctic sea ice from calibrated dual-frequency radar freeboards. *Cryosphere* 12:3551–3564. <https://doi.org/10.5194/tc-12-3551-2018>
- Laxon SW, Peacock N, Smith D (2003) High interannual variability of sea ice thickness in the Arctic region. *Nature* 425(6961):947–950
- Laxon SW, Giles KA, Ridout AL, Wingham DJ, Willatt R, Cullen R, Kwok R, Schweiger A, Zhang J, Haas C, Hendricks S, Krishfield R, Kurtz N, Farrell SL, Davidson M (2013) CryoSat estimates of Arctic Sea Ice volume. *GRL* 40(4):732–737. <https://doi.org/10.1002/grl.50193>
- Li M, Zhao C, Zhao Y, Wang Z, Shi L (2016) Polar sea ice monitoring using HY-2A scatterometer measurements. *Remote Sens* 8:688. <https://doi.org/10.3390/rs8080688>
- Lindell B, Long DG (2016) Multiyear Arctic sea ice classification using ASCAT and SSMIS. *Remote Sens* 8(4):294. <https://doi.org/10.3390/rs8040294>
- Liu WT (2003) Satellite remote sensing – surface wind. Encyclopedia of atmospheric sciences. Elsevier, Amsterdam. <https://doi.org/10.1016/B0-12-227090-8/00359-6>
- Liu AK, Zhao Y, Wu SY (1999) Arctic sea ice drift from wavelet analysis of NSCAT and special sensor microwave imager data. *J Geophys Res Ocean* 104:11529–11538. <https://doi.org/10.1029/1998JC900115>

- Lohse J, Doulgeris AP, Dierking W (2020) Mapping sea ice types from Sentinel-1 considering the surface-type dependent effect of incidence angle. *Ann Glaciol*. <https://doi.org/10.1017/aog.2020.45>
- Long D, Ulaby F (2015) Microwave radar and radiometric remote sensing. University of Michigan Press, Ann Arbor, p 930
- Lu J, Heygster G, Spreen G (2018) Atmospheric correction of sea ice concentration retrieval for 89 GHz AMSR-E Observations. *IEEE J-STARS* 11(5):1442–1457. <https://doi.org/10.1109/JSTARS.2018.2805193>
- Lu J, Heygster G, Spreen G, Scarlat R (2022) Reducing weather influences on sea ice concentration retrieval at 89 GHz using passive microwave observations. *J Geophys Res Oceans* 127:e2019JC015912. <https://doi.org/10.1029/2019JC015912>
- Maaß N, Kaleschke L, Tian-Kunze X, Drusch M (2013) Snow thickness retrieval over thick Arctic sea ice using SMOS satellite data. *Cryosphere* 7:1971–1989
- Markus T, Cavalieri DJ (1998) Snow Depth distribution over sea ice in the Southern Ocean from satellite passive microwave data. In: Jeffries MO (ed) *Antarctic Sea ice physical processes, interactions and variability*, antarctic research series, vol 74. AGU, Washington. <https://doi.org/10.1029/AR074p0019>
- Markus T et al (2017) The Ice, Cloud, and land Elevation Satellite-2 (ICESat-2): science requirements, concept, and implementation. *Remote Sens Environ* 190:260–273
- Mchedlishvili A, Spreen G, Melsheimer C, Huntemann M (2022) Weddell Sea polynya analysis using SMOS-SMAP apparent sea ice thickness retrieval. *Cryosphere* 16:471–487. <https://doi.org/10.5194/tc-16-471-2022>
- Melsheimer C, Spreen G, Ye Y, Shokr M (2022) Antarctic sea ice types from active and passive microwave remote sensing. *Cryosph Discuss*. <https://doi.org/10.5194/tc-2021-381>
- Nandan V, Geldsetzer T, Yackel J, Mahmud M, Scharien R, Howell S, King J, Ricker R, Else B (2017) Effect of snow salinity on CryoSat-2 Arctic first-year sea ice freeboard measurements. *Geophys Res Lett* 44:10419–10426. <https://doi.org/10.1002/2017GL074506>
- Nicolaus M, Perovich DK, Spreen G et al (2022) Overview of the MOSAiC expedition: snow and Sea Ice. *Elementa Sci Anth* 10(1):00046. <https://doi.org/10.1525/elementa.2021.000046>
- Ólason E, Boutin G, Korosov A, Rampal P, Williams T, Kimmritz M et al (2022) A new brittle rheology and numerical framework for large-scale sea-ice models. *J Adv Model Earth Syst* 14:e2021MS002685
- Patilea C, Heygster G, Huntemann M, Spreen G (2019) Combined SMAP/SMOS thin sea ice thickness retrieval. *Cryosphere* 13:675–691. <https://doi.org/10.5194/tc-13-675-2019>
- Paul S, Hendricks S, Ricker R, Kern S, Rinne E (2018) Empirical parametrization of Envisat freeboard retrieval of Arctic and Antarctic sea ice based on CryoSat-2: progress in the ESA Climate change initiative. *Cryosphere* 12:2437–2460. <https://doi.org/10.5194/tc-12-2437-2018>
- Peacock NR, Laxon SW (2004) Sea surface height determination in the Arctic Ocean from ERS altimetry. *J Geophys Res Oceans* 109(C7):C07001
- Perovich D, Meier W, Tschudi M, Hendricks S, Petty AA, Divine D, Farrell SL, Gerland S, Haas C, Kaleschke L, Pavlova O, Ricker R, Tian-Kunze X, Webster M, Wood K (2020) Sea ice. *Arctic Report Card 2020*. Thoman RL, Richter-Menge J, Druckenmiller ML, (Eds), <https://doi.org/10.25923/n170-9h57>
- Petty AA, Webster M, Boisvert L, Markus T (2018) The NASA Eulerian Snow on Sea Ice Model (NESOSIM) v1.0: initial model development and analysis. *Geosci Model Dev* 11:4577–4602. <https://doi.org/10.5194/gmd-11-4577-2018>
- Rampal P, Weiss J, Marsan D (2009) Positive trend in the mean speed and deformation rate of Arctic sea ice, 1979–2007. *J Geophys Res Ocean* 114:C05013. <https://doi.org/10.1029/2008JC005066>
- Rampal P, Bouillon S, Olason E, Morlighem M (2016) NeXtSIM: a new Lagrangian sea ice model. *Cryosphere* 10(3):p1055–1073. <https://doi.org/10.5194/tc-10-1055-2016>
- Rampal P, Dansereau V, Olason E, Bouillon S, Williams T, Korosov A, Samaké A (2019) On the multifractal scaling properties of sea ice deformation. *Cryosphere* 13:2457–2474. <https://doi.org/10.5194/tc-13-2457-2019>
- Ricker R, Hendricks S, Girard-Ardhuin F, Kaleschke L, Lique C, Tian-Kunze X, Nicolaus M, Krumpfen T (2017a) Satellite-observed drop of Arctic sea ice growth in winter 2015/2016. *Geophys Res Lett* 44:3236–3245. <https://doi.org/10.1002/2016GL072244>
- Ricker R, Hendricks S, Kaleschke L, Tian-Kunze X, King J, Haas C (2017b) A weekly Arctic sea-ice thickness data record from merged CryoSat-2 and SMOS satellite data. *Cryosphere* 11:1607–1623. <https://doi.org/10.5194/tc-11-1607-2017>
- Ricker R, Girard-Ardhuin F, Krumpfen T, Lique C (2018) Satellite-derived sea-ice export and its impact on Arctic ice mass balance. *Cryosphere* 12(9):3017–3032. <https://doi.org/10.5194/tc-2018-6>
- Rostovsky P, Spreen G, Farrell SL, Frost T, Heygster G, Melsheimer C (2018) Snow depth retrieval on Arctic sea ice from passive microwave radiometers—Improvements and extensions to multiyear ice using lower frequencies. *J Geophys Res Oceans* 123(10):7120–7138. <https://doi.org/10.1029/2018JC014028>

- Rousset C, Vancoppenolle M, Madec G, Fichefet T, Flavoni S, Barthélemy A, Benshila R, Chanut J, Levy C, Masson S, Vivier F (2015) The Louvain-La-Neuve sea ice model LIM3.6: global and regional capabilities. *Geosci Model Dev* 8:2991–3005. <https://doi.org/10.5194/gmd-8-2991-2015>
- Sakov P, Counillon F, Bertino L, Lisæter KA, Oke PR, Korabelv A (2012) TOPAZ4: an ocean-sea ice data assimilation system for the North Atlantic and Arctic. *Ocean Sci* 8:633–656. <https://doi.org/10.5194/os-8-633-2012>
- Sallila H, Farrell SL, McCurry J, Rinne E (2019) Assessment of contemporary satellite sea ice thickness products for Arctic sea ice. *Cryosphere* 13(4):1187–1213. <https://doi.org/10.5194/tc-13-1187-2019>
- Scarlat RC, Spreen G, Heygster G, Huntemann M, Patilea C, Toudal Pedersen L, Saldo R (2020) Sea Ice and atmospheric parameter retrieval from satellite microwave radiometers: synergy of AMSR2 and SMOS compared with the cimr candidate mission. *J Geophys Res Oceans* 125(3):e2019JC015749. <https://doi.org/10.1029/2019JC015749>
- Schmitt A, Kaleschke L (2018) A consistent combination of brightness temperatures from SMOS and SMAP over Polar Oceans for sea ice applications. *Remote Sens* 10:553. <https://doi.org/10.3390/rs10040553>
- Skourup H, Farrell SL, Hendricks S, Ricker R, Armitage TWK, Ridout A, Andersen OB, Haas C, Baker S (2017) An assessment of state-of-the-art mean sea surface and geoid models of the Arctic Ocean: implications for sea ice freeboard retrieval. *J Geophys Res Oceans*. <https://doi.org/10.1002/2017JC013176>
- Smith GC, Allard R, Babin M, Bertino L, Chevallier M, Corlett G, Crout J, Davidson F, Delille B, Gille ST, Hebert D, Hyder P, Intrieri J, Lagunas J, Larnicol G, Kaminski T, Kater B, Kaufer F, Marec C, Mazloff M, Metzger EJ, Mordy C, O'Carroll A, Olsen SM, Phelps M, Posey P, Prandi P, Rehm E, Reid P, Rigor I, Sandven S, Shupe M, Swart S, Smedstad OM, Solomon A, Storto A, Thibaut P, Toole J, Wood K, Xie J, Yang Q, The WWRP PPP Steering Group (2019) Polar Ocean observations: a critical gap in the observing system and its effect on environmental predictions from hours to a season. *Front Mar Sci* 6:429. <https://doi.org/10.3389/fmars.2019.00429>
- Spreen G, Kaleschke L, Heygster G (2008) Sea ice remote sensing using AMSR-E 89-GHz channels. *J Geophys Res* 113:C02S03. <https://doi.org/10.1029/2005JC003384>
- Spreen G, Kwok R, Menemenlis D (2011) Trends in Arctic sea ice drift and role of wind forcing: 1992–2009. *Geophys Res Lett* 38:L19501. <https://doi.org/10.1029/2011GL048970>
- Spreen G, de Steur L, Divine D, Gerland S, Hansen E, Kwok R (2020) Arctic sea ice volume export through Fram strait from 1992 to 2014. *J Geophys Res Ocean*. <https://doi.org/10.1029/2019JC016039>
- Stroeve JC, Markus T, Boisvert L, Miller J, Barrett A (2014) Changes in Arctic melt season and implications for sea ice loss. *Geophys Res Lett* 41(4):1216–1225. <https://doi.org/10.1002/2013GL058951>
- Stroeve JC, Liston GE, Buzzard S, Zhou L, Mallett R, Barrett A, Tschudi M, Tsamados M, Itkin P, Stewart JS (2020) A lagrangian snow evolution system for sea ice applications (SnowModel-LG): Part II – analyses. *J Geophys Res Oceans* 125:e2019JC015900. <https://doi.org/10.1029/2019JC015900>
- Stroeve JC, Nandan V, Willatt R, Tonboe R, Hendricks S, Ricker R, Mead J, Huntemann M, Itkin P, Schneebeli M, Krampe D, Spreen G, Wilkinson J, Matero I, Hoppmann M, Mallett R, Tsamados M (2020b) Surface-Based Ku- and Ka-band Polarimetric Radar for Sea Ice Studies (preprint). *Sea Ice/sea Ice*. <https://doi.org/10.5194/tc-2020-151>
- Svendsen E, Matzler C, Grenfell TC (1987) A model for retrieving total sea ice concentration from a spaceborne dual-polarized passive microwave instrument operating near 90 GHz. *Int J Rem Sens* 8(10):1479–1487
- Swan AM, Long DG (2012) Multiyear Arctic sea ice classification using QuikSCAT. *Trans on Geosci Remote Sens* 50(9):3317–3326. <https://doi.org/10.1109/TGRS.2012.2184123>
- Tian-Kunze X, Kaleschke L, Maaß N, Mäkynen M, Serra N, Drusch M, Krumpen T (2014) SMOS-derived thin sea ice thickness: algorithm baseline, product specifications and initial verification. *Cryosphere* 8:997–1018. <https://doi.org/10.5194/tc-8-997-2014>
- Ulaby F, Moore RK, Fung AK (1986) Microwave remote sensing: Active and passive. Volume 3 – From theory to applications. In: Theory to applications, Addison-Wesley, vol 997 pp 1986
- Wagner PM, Hughes N, Bourbonnais P, Stroeve J, Rabenstein L, Bhatt U, Little J, Wiggins H, Fleming A (2020) Sea-ice information and forecast needs for industry maritime stakeholders. *Polar Geogr* 43(2–3):160–187. <https://doi.org/10.1080/1088937X.2020.1766592>
- Wakabayashi H, Matsuoka T, Nakamura K, Nisho F (2004) Polarimetric characteristics of sea ice in the Sea of Okhotsk observed by airborne L-band SAR. *IEEE Trans Geosci Remote Sens*. <https://doi.org/10.1109/TGRS.2004.836259>
- Warren SG, Rigor IG, Untersteiner N, Radionov VF, Bryazgin NN, Aleksandrov YI, Colony R (1999) Snow depth on Arctic Sea Ice. *J Climate* 12(6):1814–1829
- Williams T, Korosov A, Rampal P, Ólason E (2021) Presentation and evaluation of the Arctic sea ice forecasting system neXtSIM-F. *Cryosphere* 15:3207–3227. <https://doi.org/10.5194/tc-15-3207-2021>

- WMO (2014) WMO Sea-Ice Nomenclature, WMO No. 259, 1: 121
- Xie J, Counillon F, Bertino L (2018) Impact of assimilating a merged sea-ice thickness from CryoSat-2 and SMOS in the Arctic reanalysis. *Cryosphere* 12(11):3671–3691
- Ye Y, Shokr M, Heygster G, Spreen G (2016) Improving multiyear ice concentration estimates with ice drift. *Remote Sens* 8(5):397. <https://doi.org/10.3390/rs8050397>
- Yi D and Zwally HJ (2009). Arctic Sea Ice Freeboard and Thickness, Version 1 [Data Set]. NASA National Snow and Ice Data Center Distributed Active Archive Center. Boulder, Colorado. <https://doi.org/10.5067/SXJVJ3A2XIZT>
- Yitayew TG, Dierking W, Divine DV, Eltoft T, Ferro-Famil L, Rösel A, Negrel J (2018) Validation of sea-ice topographic heights derived from TanDEM-X interferometric SAR data with results from laser profiler and photogrammetry. *IEEE Trans Geosci Remote Sens* 56(11):6504–6520. <https://doi.org/10.1109/TGRS.2018.2839590>
- Zhou L, Stroeve J, Xu S, Petty A, Tilling R, Winstrup M, Rostosky P, Lawrenc IR, Liston GE, Ridout A, Tsamados M, Nandan V (2021) Inter-comparison of snow depth over Arctic sea ice from reanalysis reconstructions and satellite retrieval. *The Cryosph* 15:345–367. <https://doi.org/10.5194/tc-15-345-2021>

Publisher's Note Springer Nature remains neutral with regard to jurisdictional claims in published maps and institutional affiliations.

Authors and Affiliations

Stein Sandven¹  · Gunnar Spreen²  · Georg Heygster³  · Fanny Girard-Ardhuin⁴  · Sinéad L. Farrell⁵  · Wolfgang Dierking^{6,7}  · Richard A. Allard⁸ 

Gunnar Spreen
gunnar.spreen@uni-bremen.de

Georg Heygster
heygster@uni-bremen.de

Fanny Girard-Ardhuin
fanny.ardhuin@ifremer.fr

Sinéad L. Farrell
sineadf@umd.edu

Wolfgang Dierking
Wolfgang.Dierking@awi.de

Richard A. Allard
Richard.allard@nrlssc.navy.mil

- ¹ Nansen Environmental and Remote Sensing Center, Jahnebakken 3, 5007 Bergen, Norway
- ² Institute of Environmental Physics, University of Bremen, 28359 Bremen, Germany
- ³ GEORG-Lab and Institute of Environmental Physics, University of Bremen, 28359 Bremen, Germany
- ⁴ Ifremer, UBO, CNRS, IRD, Laboratoire d'Océanographie Spatiale (LOPS), IUEM, 29280 Plouzané, France
- ⁵ Department of Geographical Sciences, University of Maryland, College Park, MD 20742, USA
- ⁶ Alfred Wegener Institute, Helmholtz Centre for Polar and Marine Research, 27570 Bremerhaven, Germany
- ⁷ University of Tromsø, the Arctic University of Norway, 9019 Tromsø, Norway
- ⁸ Ocean Sciences Division, U. S. Naval Research Laboratory, Stennis Space Center, Hancock County, MS 39529, USA